Global Biogeochemical Cycles

RESEARCH ARTICLE
10.1029/2019GB006456

Spatiotemporal Variability in Modeled Bottom Ice and Sea Surface Dimethylsulfide Concentrations and Fluxes in the Arctic During 1979–2015

Hakase Hayashida[1,2], Gauthier Carnat[3], Martí Galí[4], Adam H. Monahan[1], Eric Mortenson[1,5], Tessa Sou[6], and Nadja S. Steiner[6]

[1]School of Earth and Ocean Sciences, University of Victoria, Victoria, British Columbia, Canada, [2]Institute for Marine and Antarctic Studies, University of Tasmania, Hobart, Tasmania, Australia, [3]Laboratoire de Glaciologie, Université Libre de Bruxelles, Brussels, Belgium, [4]Department of Earth Sciences, Barcelona Supercomputing Center, Barcelona, Spain, [5]CSIRO Marine and Atmospheric Research, Hobart, Tasmania, Australia, [6]Institute of Ocean Sciences, Fisheries and Oceans Canada, Sidney, British Columbia, Canada

Abstract Field observations suggest that oceanic emissions of dimethylsulfide (DMS) may play a dominant role in the production of Arctic aerosols and clouds and therefore modulate the surface irradiance, during spring and summer. DMS is produced not only in the water column but also in various sea ice habitats. The ongoing recession of Arctic sea ice is expected to enhance DMS emissions, but the magnitude of this increase is highly uncertain. Here we investigate the spatiotemporal variability in bottom ice and sea surface DMS concentrations and fluxes using a regional sea ice-ocean physical-biogeochemical model. Model results indicate that the observed accelerated decline of Arctic sea ice extent since the beginning of the 21st century is associated with upward trends in May–August pan-Arctic-averaged sea surface DMS concentration and sea-to-air DMS flux. On the other hand, strong interannual variability and statistically insignificant trends are found for bottom ice DMS concentration and ice-to-sea DMS flux, owing to the counteracting effects of the shrinking horizontal extent and the vertical thinning of sea ice on ice algal production. The pan-Arctic DMS climatology products based on model simulation and satellite algorithms provide dynamically based spatial details that are absent in the in situ measurement-based climatology due to limited spatiotemporal data coverage and inevitable extrapolation bias. Lastly, model results indicate that the bottom ice DMS and its precursor dimethylsulfoniopropionate production can be the only local source of oceanic DMS emissions into the atmosphere during May prior to pelagic blooms, suggesting that it may be a key component of the biological control on Arctic climate at that time.

Key Points:
- Model results reveal a 39% increase in the May–August and pan-Arctic mean sea-to-air DMS flux since the beginning of the 21st century
- In contrast, bottom ice DMS shows no apparent trend but exhibits strong interannual variability
- Bottom ice DMSP and DMS can become the sole source of sea surface DMS concentration and sea-to-air flux over extended regions in May

Supporting Information:
- Supporting Information S1

Correspondence to:
H. Hayashida,
hakase.hayashida@utas.edu.au

Citation:
Hayashida, H., Carnat, G., Galí, M., Monahan, A. H., Mortenson, E., Sou, T., & Steiner, N. S. (2020). Spatiotemporal variability in modeled bottom ice and sea surface dimethylsulfide concentrations and fluxes in the Arctic during 1979–2015. *Global Biogeochemical Cycles*, *34*, e2019GB006456. https://doi.org/10.1029/2019GB006456

Received 18 OCT 2019
Accepted 5 OCT 2020
Accepted article online 9 OCT 2020

1. Introduction

Dimethylsulfide (DMS) is the most abundant volatile sulfur compound in the ocean (Sim, 2001). DMS is produced by the enzymatic cleavage of dimethylsulfoniopropionate (DMSP), which is an osmolyte produced mainly by marine algae (Stefels et al., 2007). Oceanic emissions of DMS are the main source of biogenic aerosols, playing an important role in radiative forcing and atmospheric chemistry (Andreae & Crutzen, 1997). Recent observational studies suggest that sea-to-air DMS flux may exert a strong influence on Arctic climate during late spring and summer by playing a dominant role in aerosol composition and new particle formation in the region (Chang et al., 2011; Ghahremaninezhad et al., 2016; Mungall et al., 2016; Rempillo et al., 2011; Sharma et al., 2012; Park et al., 2017; Willis et al., 2016). However, these studies are limited both spatially and temporally, and therefore, the extent to which their conclusions scale up to the broad Arctic domain remains unknown.

One of the main challenges in Arctic DMS research is the poor spatiotemporal coverage of sea surface DMS concentration measurements; direct measurements in ice-covered regions are logistically difficult, while indirect measurements via remote sensing are restricted to open water (where ice concentration is less than 10% Gal et al., 2019) and are not available near the North Pole. As a result, the existing climatologies of sea surface DMS concentration for the Arctic domain have been primarily constructed either by the extrapolation of in situ measurements from lower latitudes (Kettle & Andreae, 2000; Kettle et al., 1999; Lana et al., 2011) or machine learning (Humphries et al., 2012). Given the spatial heterogeneity of sea

surface DMS concentration in the Arctic (Levasseur, 2013), such an approach to producing the sea surface DMS concentration fields that feed into atmospheric, global climate, and Earth system models is potentially problematic.

Another approach to obtain sea surface DMS concentration fields is via numerical modeling. Process models apply mechanistic representations of key physical and biogeochemical processes to produce simulations over time periods and spatial domains that are beyond the capacity of field observations. Only a handful of papers in the literature focus on modeling DMSP and DMS production in the Arctic Ocean (Elliott et al., 2012; Gabric et al., 1999, 2005; Hayashida et al., 2017; Jodwalis et al., 2000; Qu et al., 2016; Qu & Gabric, 2010). Elliott et al. (2012) are notable as the only study that incorporated sea ice biogeochemistry into a regional model framework and therefore could address the spatial variability in sea surface DMS concentration. However, this earlier study did not address the temporal variability in sea surface DMS concentration nor quantify the impacts of sea ice biogeochemistry on the sea-to-air DMS flux.

The decline of Arctic sea ice extent and thickness is one of the most striking consequences of ongoing climate change and has implications for oceanic DMS emissions. Using a zero-dimensional box model, Gabric et al. (2005) projected an 86% increase in sea-to-air DMS flux in the Barents Sea between the late 20th and the 21st centuries, owing to both substantial loss of ice cover and ocean warming (with consequent reduction in the gas solubility). Similarly, future climate projections using an Earth system model (Six et al., 2013) suggest that oceanic DMS emissions will increase in the Arctic north of 60°N, while a reduction is projected for the lower latitudes. However, these earlier studies either focused on a confined region in the Arctic (Gabric et al., 2005) or were global analyses with limited focus on the Arctic (Six et al., 2013). Furthermore, the spatial resolution of the global model used in Six et al. (2013) might be inadequate to resolve fine-scale processes near the sea ice-ocean interface (Hayashida et al., 2019). Most recently, a 2.4-fold increase in ocean DMS emissions north of 70°N is predicted for the ice-free Arctic summer compared to the present-day climatology based on a remote sensing algorithm, although this trend may diverge due to regime shifts in Arctic ecosystems in coming decades (Gal et al., 2019).

In the present study, we investigate the spatiotemporal variability in bottom ice and sea surface DMS concentrations and fluxes in the Arctic using a three-dimensional regional coupled sea ice-ocean physical-biogeochemical model. Specific objectives of this study include (1) an assessment of the temporal variability in sea ice and sea surface physical and biogeochemical properties over 1979–2015, (2) a comparison of the model-based pan-Arctic sea surface DMS climatology with previous climatologies based on satellite observations and in situ measurements, and (3) a quantification of the contribution of bottom ice DMSP and DMS production to sea surface DMS concentration and sea-to-air flux. In the following, we describe the model and the evaluation data products in section 2, present the results of model simulations and evaluation in section 3, discuss the key findings in section 4, and provide conclusions in section 5.

2. Methods

2.1. Pan-Arctic Model Configuration

We used a pan-Arctic configuration of the sea ice-ocean coupled general circulation model based on the Nucleus for European Modelling of Ocean (NEMO) version 3.4 (Hayashida et al., 2019). The coupled model consists of physical and biogeochemical components. The physical component is comprised of the Océan PArallélisé (OPA) free surface hydrostatic primitive equation ocean model (Madec, 2008) coupled to a three-layer (one for snow and two for ice) dynamic-thermodynamic sea ice model called the Louvain-la-Neuve Sea Ice Model version 2 (LIM2; Bouillon et al., 2009; Fichefet & Maqueda, 1997). The biogeochemical component is comprised of the Canadian Ocean Ecosystem model (CanOE) coupled to the Canadian Sea Ice Biogeochemistry model (CSIB; Hayashida et al., 2019). We refer to the CSIB-CanOE biogeochemical component presented in this study as version 4 (CSIBv4), as a few modifications were made from the previous version (detailed below). The pan-Arctic configuration covers the entire Arctic, the North Atlantic north of approximately 50°N, and the North Pacific north of approximately 60°N, with the exception of Hudson Bay. The configuration has been applied to study the projected changes in sea ice conditions and freshwater fluxes in the Canadian Polar Shelf (Hu & Myers, 2014) and has recently been updated with finer vertical resolution in the upper water column to better represent the effects of meltwater on both physical and biogeochemical processes (Hayashida et al., 2019). The horizontal resolution of the ocean model varies

from 10–14.5 km, while the updated vertical resolution varies from 1–255 m, with 12 levels (of thickness 1, 2, 2, 3, 4, 5, 6, 8, 10, 13, 16, and 20 m) in the upper 90 m (Hayashida et al., 2019).

CanOE is a nutrient-phytoplankton-zooplankton-detritus (NPZD) ecosystem model with a representation of carbonate chemistry, originally developed for use in the Canadian Earth System Model version 5 (Swart et al., 2019). Key features of CanOE include representations of small and large size classes for each of phytoplankton, zooplankton, and detritus and variable stoichiometric ratios for phytoplankton (carbon, nitrogen, iron, and chlorophyll). In Hayashida et al. (2019), CanOE was implemented into the pan-Arctic configuration with additional state variables (DMSP and DMS) and coupling to CSIB. CSIB is a five-state variable (nitrogen, ammonium, ice algae, DMSP, and DMS) model that simulates biogeochemical processes at the bottom layer of sea ice where ice algal production within sea ice typically dominates (Meiners et al., 2018). The bottom layer thickness is fixed to 3 cm in our study. In addition to biogeochemical sources and sinks, the state variables follow the horizontal sea ice motion and ocean circulation governed by the advection-diffusion equations and are exchanged at the ice-ocean interface through turbulent and molecular diffusion, ice growth/melt, and freshwater flushing (Hayashida et al., 2019). Furthermore, the biogeochemical tracer concentrations in the uppermost ocean layer vary with freshwater flux.

The DMSP and DMS model components consist of bottom ice and seawater representations and are based on ones developed within a one-dimensional framework (Hayashida et al., 2017). DMSP is separated into particulate (DMSPp) and dissolved (DMSPd) phases for both sea ice and ocean compartments. In total, six model equations represent the budgets of bottom ice DMSPp, bottom ice DMSPd, bottom ice DMS, seawater DMSPp, seawater DMSPd, and seawater DMS. All of these quantities are modeled in terms of their concentrations with units of μmol m^{-3}. DMSPp is an osmolyte produced in many species of marine algae and plants (Stefels, 2000). The amount of DMSPp produced relative to carbon biomass varies considerably among algal species and also depends on environmental conditions (Stefels et al., 2007). In many extrapolar regions, diatoms are found to be low DMSP producers, whereas dinoflagellates and haptophytes are high DMSP producers (Stefels et al., 2007). However, in polar regions, diatoms exhibit intracellular DMSP-to-carbon (chlorophyll *a*) ratios that are substantially higher than open-ocean diatoms (Galindo et al., 2014), likely due to their additional role as cryoprotectant (Kirst et al., 1991). Furthermore, polar diatoms accumulate in very high concentrations at the base of and underneath the sea ice, resulting in elevated production of DMSP (Galindo et al., 2014). In the model, the intracellular DMSP-to-carbon ratio for small phytoplankton is set to 12 mmol S:mol C, which is representative of haptophytes (Stefels et al., 2007). The ratios for ice algae and large phytoplankton are set to 4 mmol S:mol C, which is representative of polar diatoms (see Appendix A). This ratio is about 4 times higher than that of extrapolar diatoms (Stefels et al., 2007). DMSPp is released outside of algal cells as DMSPd through cell lysis and exudation. DMSPd is converted to DMS by bacteria and free DMSP-lyase enzymes. DMSPp, DMSPd, and DMS produced within the bottom ice are released into surface ocean where DMS may be emitted into the atmosphere. A full description of the model equations and parameters is provided in Appendix A and supporting information.

In this study, we made a few modifications to the configuration of Hayashida et al. (2019) to improve the simulation of physical and biogeochemical processes. First, we prescribed river runoff of nitrate, total alkalinity, and dissolved organic and inorganic carbon by constructing their annual mean concentration fields based on in situ measurements from major Arctic rivers (Figure S1 and Table S1), as opposed to setting these fields to zero in the previous study. Second, we removed the dependence of phytoplankton and zooplankton source and sink terms on iron concentration to avoid spurious reductions in their respective biomass that may arise due to the lack of external supply (dust deposition and river input) of dissolved iron in the current model setup. In practice, this change was achieved by setting the dissolved iron concentration to a high value (0.6 nM) everywhere in the model domain at every model time step. The change has a negligible effect on the results of Hayashida et al. (2019) given the short span of the simulations but was deemed necessary for the multidecadal simulation carried out in the present study. This change is also justified in part by the fact that iron is generally not the limiting factor for phytoplankton growth for the Arctic domain (Aumont et al., 2003, 2015; Zahariev et al., 2008). Third, we removed the effect of nutrient stress on the DMSP content of small phytoplankton as Stefels et al. (2007) and McParland and Levine (2019) suggested that the DMSP production of high DMSP-producing algae, such as small phytoplankton in the present study, is not affected much by nutrient limitation. Fourth, we changed the values of the following model parameters from the values used in Hayashida et al. (2019) in order to further tune the modeled ice volume and extent: the thickness of newly formed ice (*hiccrit*; from 0.6 to 0.5 m) and the ice strength parameter (*pstar*; from

23,000 to 30,000 N m^{-2}). Our preliminary simulations indicated that the modeled ice volume and extent were directly proportional to *hiccrit* within the range 0.3–0.8 m, and the modeled ice extent was inversely proportional to *pstar*, while the modeled ice volume was insensitive to the choice of *pstar* within the range 23,000–45,000 N m^{-2}.

With these changes, we conducted a 47 year simulation from 1 January 1969 to 31 December 2015 by prescribing annually varying surface and lateral boundary conditions forced with the Drakkar Forcing Set version 5.2 (Figure S2 Dussin et al., 2016) and the Ocean Reanalysis System 4 (Figure S3; Balmaseda et al., 2013). The model state variables were initialized as described in Hayashida et al. (2019) and saved as monthly mean fields. We considered the first 10 years of the simulation as a spin-up phase for sea ice and sea surface variables (Hayashida et al., 2019) and focused the analysis on the latter 37 years (1979–2015).

To quantify the contribution of bottom ice DMSP and DMS production to sea surface DMS concentration and sea-to-air DMS flux, we conducted an additional simulation that excludes the model representation of bottom ice DMSP and DMS production. The additional simulation spanned 10 years (2006–2015) initialized from the state at the end of 2005 in the 47 year simulation. No spin-up was necessary for this simulation as the bottom ice production had only seasonal influence on sea surface DMS concentration.

2.2. Data Products for Model Evaluation

2.2.1. Pan-Arctic Ice Ocean Modeling and Assimilation System

The Pan-Arctic Ice Ocean Modeling and Assimilation System (PIOMAS) is a regional coupled sea ice-ocean circulation model that assimilates observational data (Schweiger et al., 2011; Zhang & Rothrock, 2003). The monthly mean fields of snow depth, ice thickness, and ice concentration simulated by PIOMAS version 2.1 were used to create time series of snow volume, ice volume, and ice extent integrated over the domain north of 60°N.

2.2.2. Sea Ice Index Version 3 (NSIDC)

The National Snow and Ice Data Center (NSIDC) provides ice extent data derived from multiple satellite sensors known as the Sea Ice Index Version 3 (Data set ID: G02135; Fetterer et al., 2017). We obtained the monthly mean time series of sea ice extent in the Arctic to compare with the modeled September mean ice extent time series over 1979–2015.

2.2.3. World Ocean Atlas 2018

The World Ocean Atlas (WOA) of the National Oceanic and Atmospheric Administration provides climatological fields of oceanic properties based on in situ measurements. We obtained the monthly and annual mean fields of sea surface nitrate concentration of the latest version 2018 (WOA18) that incorporate biogeochemical Argo float measurements (Riser et al., 2016) and the Global Ocean Data Analysis Project version 2 (GLODAPv2; Lauvset et al., 2016). To the best of our knowledge, WOA18 is the only existing in situ measurement-based data product that provides globally interpolated nitrate fields at monthly temporal resolution. However, the data incorporated into WOA18 have substantial spatiotemporal gaps for the Arctic domain, and therefore, their climatological fields need to be interpreted with caution. For example, the spatial coverage of measurements incorporated into the monthly interpolated fields is extremely scarce (5–26% over the pan-Arctic domain; Figure S4), indicating that their interpolated fields heavily rely on extrapolation of measurements from lower latitudes. Furthermore, these fields do not represent strictly the temporal mean over the nominal averaging period due to missing values in some years. The nitrate concentration of WOA18 is given in μmol kg^{-1}, which is multiplied by the WOA18 seawater density climatology to convert to the model units (mmol m^{-3})

2.2.4. The Carnat 2013 (C13) Bottom Ice DMS Data Set

In situ measurements of sea ice DMS concentration were conducted between November 2007 and June 2008 in the southern Beaufort Sea-Amundsen Gulf of the Canadian Arctic as part of the International Polar Year Circumpolar Flaw Lead (IPY-CFL) system study (Carnat et al., 2013). Both physical and biogeochemical properties were measured from 33 first year drift and fast ice stations and were presented in full details in Carnat (2013). In the present study, we compared the 23 samples of DMS concentrations collected from the bottom 3 cm of sea ice with the model results. It should be acknowledged that these measurements come from multiple locations and do not represent a time series. However, as discussed in Carnat et al. (2013), the spatial variability in these measurements was minimized through careful selection of ice floes for each sampling.

2.2.5. The Galí 2019 (G19) Sea Surface DMS Climatology

For evaluation of modeled sea surface DMS concentration fields at the pan-Arctic scale, we used a monthly mean climatology product which was constructed using a remote sensing algorithm developed for the Arctic domain (G19; Gal et al., 2019). The spatial coverage of the G19 climatology is north of 45°N with a resolution of 28 km. The temporal coverage of the satellite observations incorporated into the climatology is the years 2003–2016. The algorithm for estimating sea surface DMS concentration depends on the light penetration regime, sea surface photosynthetically active radiation (PAR, that part of the shortwave irradiance available for photosynthetic production), and sea surface chlorophyll *a* concentration. The remotely sensed chlorophyll *a* signal in Arctic coastal regions may overestimate the actual concentration due to the presence of riverine colored dissolved organic matter and detritus, collectively termed colored detrital matter (CDM; Maritorena et al., 2002). To address this bias, we screened out grid cells with high CDM concentration using satellite-based climatological annual mean fields of light absorption coefficient at 412 nm as a proxy (Gal et al., 2019). Specifically, we disregarded values from grid cells shallower than 200 m in depth (i.e., coastal environment) and for which the absorption coefficient was greater than 0.25 m^{-1}. This criterion is overall conservative and is consistent with the regionalization applied by Gal et al. (2019).

2.2.6. The Lana 2011 (L11) Sea Surface D.MS Climatology

The most up-to-date global monthly mean sea surface DMS climatology product based on in situ measurements is the Lana 2011 (L11) climatology (Lana et al., 2011). The L11 climatology incorporates over 47,000 near-surface DMS concentration measurements taken during 1972–2009 to construct interpolated/extrapolated monthly mean fields at the spatial resolution of 1° on a global regular grid (Lana et al., 2011).

It is important to emphasize the fact that the Arctic representation in the L11 climatology is based on extremely limited data (0–4% areal coverage north of 60°N; Figure S5) and so relies on the extrapolation of in situ measurements from lower latitudes. The extrapolation extends into the ice-covered areas where primary production (and subsequent DMS formation) is presumably lower than the open water production due to light limitation. Despite the extrapolation bias for the Arctic, the L11 climatology deserves attention because it is commonly used for prescribing the DMS emissions in global climate and Earth system models.

2.3. Trend Analysis

The relative strength of modeled pan-Arctic mean interannual variability was assessed by comparing the magnitude of year-to-year variation with the longer-term trends determined by the LOcally WEighted Scatterplot Smoothing (LOWESS). LOWESS is a nonparameteric regression that determines a least squares polynomial fit to a time series (Cleveland, 1979). Numerically, we calculated LOWESS using the Python package statsmodels. The shapes of LOWESS curves were examined to assess the linearity of the longer-term trends. To quantify trends, linear regression of the time series was then applied over the time period in which the LOWESS curve was quasi-linear.

3. Results

3.1. Pan-Arctic Mean Time Series

To understand the temporal variability in modeled physical and biogeochemical properties at the pan-Arctic scale as a whole, we examine the seasonal and interannual variability of quantities averaged over the pan-Arctic domain defined as the region north of 60°N (sections 3.1.1 and 3.1.2, respectively) and compare these with comparable averages from other data products (section 3.1.3).

3.1.1. Seasonal Cycles

Modeled snow volume, ice volume, and ice extent increase during fall and winter, reaching annual maxima in early spring (April for snow volume and ice volume and March for ice extent; Figures 1a–1c). Seasonal warming during spring and summer results in a nearly snow-free model ice surface in July and August, while the annual minima in ice volume and extent occur in September.

Growth of ice algae is largely controlled by the amount of available light and nutrients (Gosselin et al., 1990). In the model, the influence of these two factors on the ice algal growth rate is defined as limitation indices that range from zero to one (Mortenson et al., 2017). The growth rate of modeled ice algae is directly proportional to the minimum of the two limitation indices. Much of the bottom ice is light limited from October to April, while nutrient limitation dominates from June to September (Figure 1d). In May, both factors share about the same areal extent. Modeled ice algal biomass increases gradually from February to March, rapidly

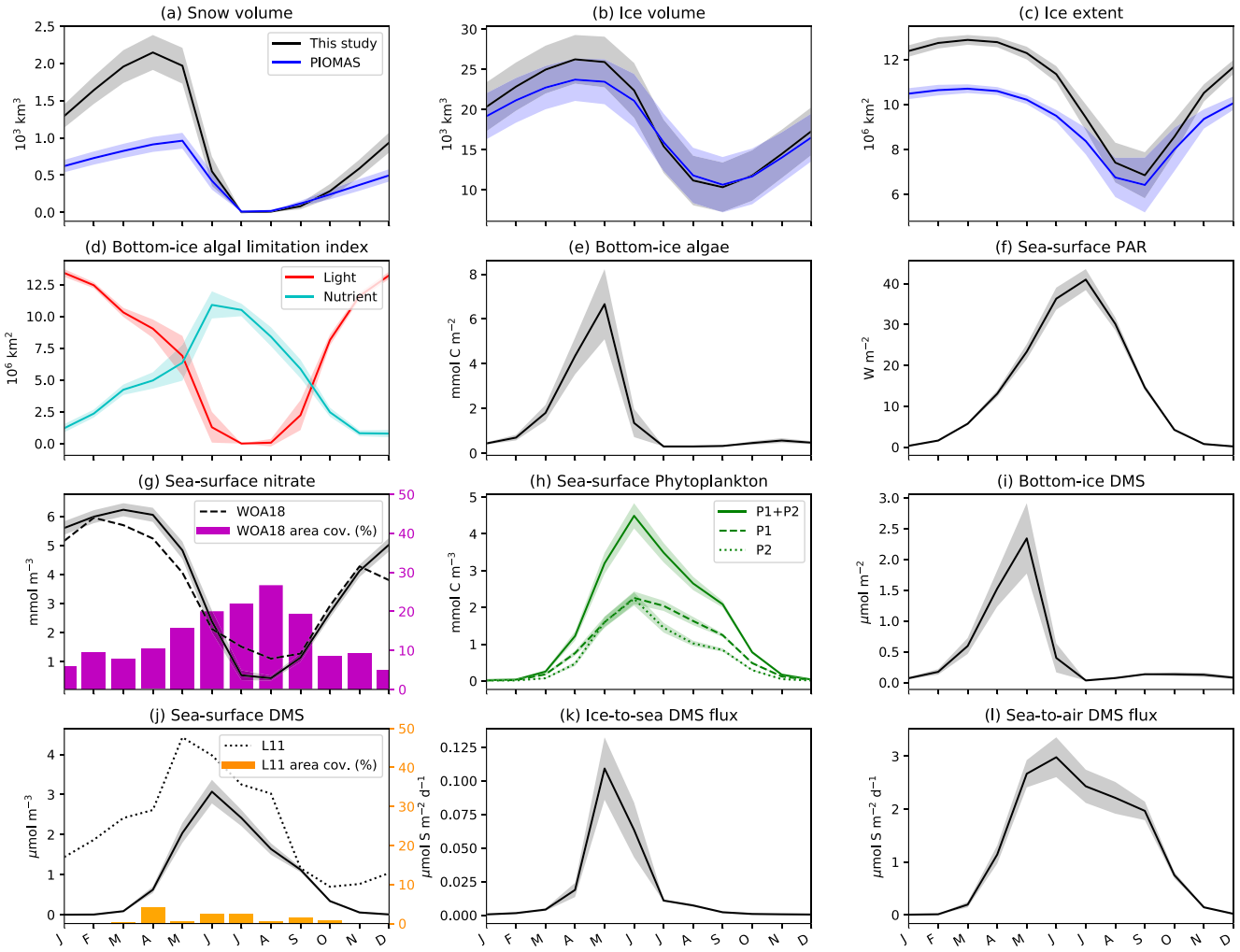

Figure 1. Modeled pan-Arctic climatological seasonal cycles and their comparisons with available data products. Panels represent the monthly mean (a) snow volume; (b) ice volume; (c) ice extent; (d) spatial extent of bottom ice that is light (red) or nutrient (cyan) limited for bottom ice algal growth; (e) bottom ice algal biomass; (f) sea surface PAR; (g) sea surface nitrate concentration; (h) sea surface biomass of small phytoplankton (dashed), large phytoplankton (dotted), and both (solid); (i) bottom ice DMS concentration; (j) sea surface DMS concentration; (k) ice-to-sea DMS flux, and (l) sea-to-air DMS flux. Subplots a–d represent spatially integrated quantities, while the others represent spatially averaged quantities over the region north of 60°N. Shaded regions represent the ±1 interannual standard deviation of monthly averaged quantities over 1979–2015. All line plots are our model results except for PIOMAS (blue lines in a–c), WOA18 (dashed line in g), and L11 (dotted line in j). Bar graphs represent the spatial extent of gridded in situ measurements north of 60°N incorporated into WOA18 (g) and L11 (j).

from March to May, and declines from May to July, after which it remains near zero except for a slight increase in November (Figure 1e). The spring bloom of modeled ice algae is largely controlled by light in its growth phase, while it is terminated by a combination of nutrient limitation and habit loss, as indicated by a co-occurrence of a sharp decline of ice algal biomass and snow/ice melting after May (Figures 1a–1c).

Modeled sea surface PAR averaged over both ice-covered and open water areas gradually increases from nearly zero during the polar night to an annual peak in July (Figure 1d). This peak coincides with the annual minimum in snow volume. Modeled sea surface nitrate concentration ranges from above 5 mmol m^{-3} during winter and early spring to below 1 mmol m^{-3} during July–August (Figure 1e). Modeled sea surface phytoplankton biomass increases from March, peaks in June, and declines during the rest of the year (Figure 1h). The biomass of small phytoplankton (P1) is similar to that of large phytoplankton (P2) from the beginning of the spring bloom to its peak. However, following the peak, the rate of decline is faster for large phytoplankton due to their higher susceptibility to nutrient limitation (Hayashida, 2018).

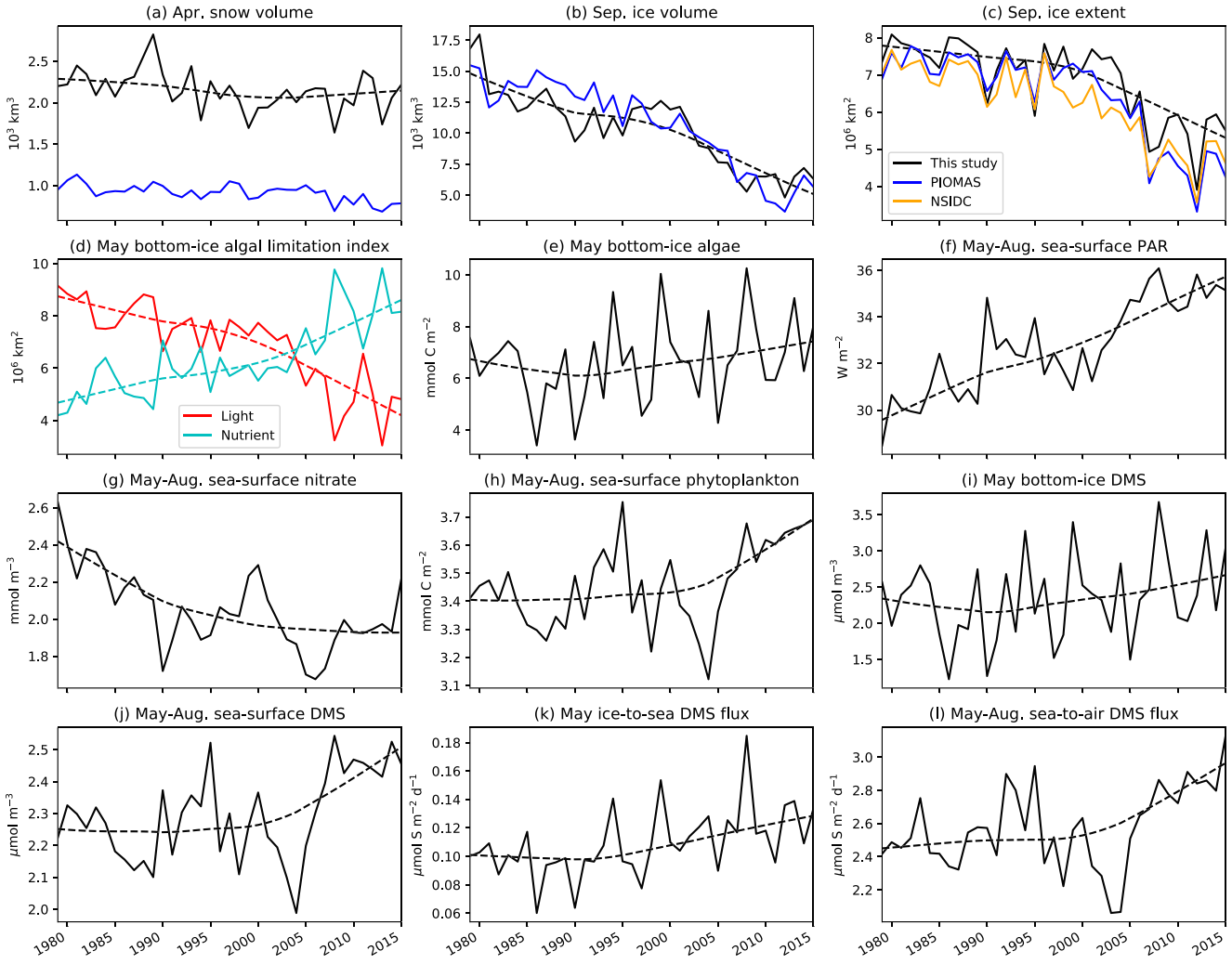

Figure 2. Modeled pan-Arctic interannual variability and trends over 1979–2015. Solid lines represent year-to-year variations in (a) April mean snow volume, (b) September mean ice volume, (c) September mean ice extent, (d) May mean spatial extent of bottom ice that is light (red) or nutrient (cyan) limited for bottom ice algal growth, (e) May mean bottom ice algal biomass, (f) May–August mean sea surface PAR, (g) May–August mean sea surface nitrate concentration, (h) May–August mean sea surface total (small and large) phytoplankton biomass, (i) May mean bottom ice DMS concentration, (j) May–August mean sea surface DMS concentration, (k) May mean ice-to-sea DMS flux, and (l) May–August mean sea-to-air DMS flux. Dashed lines represent trends determined by the LOWESS nonparametric regression. Subplots a–d represent spatially integrated quantities, while the others represent spatially averaged quantities over the region north of 60°N. Blue (a–c) and orange (c) lines represent the corresponding time series of PIOMAS and NSIDC, respectively.

The relative magnitude and timing of bottom ice and sea surface DMS concentration variations are almost identical to those of ice algal and phytoplankton biomass, respectively (Figures 1i and 1j). Modeled fluxes of DMS from the bottom ice to the sea surface (ice-to-sea) and from the sea surface to the atmosphere (sea-to-air) depend primarily on their respective bottom ice and sea surface concentrations. As such, the ice-to-sea DMS flux is at its annual maximum in May and the sea-to-air flux in June (Figures 1k and 1l). However, the changes from May to September are quite different between the sea surface DMS concentration and the sea-to-air flux. Despite the sharp decline of the sea surface DMS concentration during this time, the sea-to-air flux remains relatively high due to the seasonal maximum in open water area promoting the gas transfer. In contrast, the ice-to-sea DMS flux drops to almost zero by July.

3.1.2. Interannual Variability and Trends

Relatively strong interannual variability and weak trends are found for modeled snow volume, ice algal biomass, bottom ice DMS concentration, and ice-to-sea DMS flux (Figures 2a, 2e, 2i, and 2k). In contrast, relatively strong trends are found for other model variables, although for these quantities, interannual

variability is not necessarily negligible. For example, the decrease in phytoplankton biomass from 1995 to 1996 is large relative to the trend depicted by the LOWESS curve (Figure 2h).

Particularly noteworthy is an abrupt change in the ice extent trend at around year 2000 (Figure 2c). Specifically, the slopes of the LOWESS curve before and after 2000 are both quasi-linear but the decline in the second period is substantially more rapid. The timing of this abrupt change in the slope of the decline is consistent with the trends derived from satellite observations (Stroeve et al., 2012). Least squares regression of the pan-Arctic modeled September mean ice extent over 2001-2015 results in a linear trend of -0.17×10^6 km^2 yr^{-1} (corresponding to a 32% decrease over this period).

Abrupt changes in the LOWESS curves since the beginning of the 21st century to quasi-linear increases are also present in modeled sea surface phytoplankton biomass, sea surface DMS concentration, and sea-to-air DMS flux (Figures 2h, 2j, and 2l). The correspondence between these shifts in trend suggests a response of ocean biogeochemistry to the accelerated decline of sea ice cover. Least squares regression over 2001–2015 reveals a linear trend of 0.03 mmol C m^{-3} yr^{-1} for the May–August mean phytoplankton biomass, 0.03 μmol S m^{-3} yr^{-1} for the May–August mean DMS concentration, and 0.06 μmol S m^{-2} day^{-1} yr^{-1} for the May–August mean sea-to-air DMS flux (resulting respectively in 14%, 19%, and 39% changes over 2001–2015 period). The spatial distributions of decadal mean anomalies in these variables between before (1986–1995) and after (2006–2015) the accelerated decline of Arctic sea ice extent show strong correspondence to those of ice concentration in the first year ice and to sea surface nutrient concentration in the Central Arctic basin (Figure S6).

The slope of the LOWESS curve for modeled September mean ice volume is relatively consistent throughout 1979–2015 except for a slight decrease during the 1990s (Figure 2b). The linear trend for the ice volume over this entire period is −0.25 thousand km^3 yr^{-1}, resulting in 61% loss since 1979. The LOWESS curve for the ice volume strongly anticorrelates with that of sea surface PAR (Figure 2f), which is a result of both horizontal shrinking and vertical thinning of Arctic sea ice. Vertical thinning also relaxes light limitation for ice algal growth, resulting in a shift from light-limited to nutrient-limited regime in the pan-Arctic bottom ice ecosystem from 2005 onward (Figure 2d).

3.1.3. Comparison With Existing Data Products

PIOMAS exhibits a similarly shaped seasonal cycle of snow volume as our model results except that the annual peak is in May (Figure 1a). Additionally, snow volume is lower in PIOMAS, resulting in more than twofold difference in the annual peak value. This discrepancy is found throughout 1979–2015 (Figure 2a). However, our model simulates substantially lower snow depth than the in situ measurement-based snow climatology (Shalina & Sandven, 2018) and the satellite-based estimates over recent years (Lawrence et al., 2018). Hence, the quantitative discrepancy between our model and PIOMAS is likely due to unrealistically low snow accumulation in PIOMAS. Simulating snow depth is extremely challenging not only due to the very limited available observations but also due to the complex processes affecting snow accumulation and redistribution.

The seasonal cycles of ice volume between our model and PIOMAS match exceptionally well from June to December, while they differ by a few thousand km^3 in other months (Figure 1b). Similar results are found for ice extent, but the discrepancy is larger. Unlike the ice volume, the monthly mean ice extent in our model and PIOMAS does not overlap within the interannual standard deviation (Figure 1c). Considering interannual variability, our model simulates lower September mean ice volume between the mid-1980s and the mid-1990s but is higher since 2010 (Figure 2b). Overall, the variability is consistent with PIOMAS as indicated by strong correlation between their detrended interannual time series ($r^2 = 0.89$, $p < 0.05$). Modeled September mean ice extent is generally higher than PIOMAS and NSIDC but correlates well ($r^2 = 0.94$, $p < 0.05$ for both cases).

The seasonal cycles of sea surface nitrate concentration between our model climatology and WOA18 are similar except that the timing of the annual maximum differs by a month (March vs. February) and the summer concentration is somewhat lower in the model (up to >1 mmol m^{-3} difference in July). The range of modeled annual means over 1979–2015 (Figure 2g) is much smaller than the seasonal range and is close to the annual mean of WOA18 (3.5 mmol m^{-3}). Given the limited spatial coverage of gridded in situ measurements incorporated in WOA18 (5–26% of the north of 60°N), it is unclear to what extent differences between the model and WOA18 are due to model biases or sampling bias in WOA18.

The modeled seasonal cycle of sea surface DMS concentration shows consistently lower values than the L11 climatology (Figure 1j). The difference is 1.3 μmol m^{-3} on an annual average and exceeds 2 μmol m^{-3} in March and May. The spatial coverage of gridded in situ measurements incorporated into the L11 climatology ranges from 0–4% in the Arctic domain, and so the climatology is strongly influenced by in situ measurements from lower latitudes. In lower latitudes, phytoplankton blooms occur earlier, last longer, and emit more DMS (due to the lack of sea ice cover and higher nutrient concentrations). Inevitably, this extrapolation bias affects both the magnitude and timing of the seasonal cycle in the Arctic domain. The model suggests that the annual peak occurs a month later than indicated in the L11 climatology. Similarly, 10 out of 12 empirical and prognostic models suggest that the annual peak occurs later than May (Tesdal et al., 2016), in contradiction to the L11 climatology over the pan-Arctic domain. Although very high concentrations of ice algae and underice phytoplankton can lead to high DMSP and subsequent DMS production prior to the seasonal recession of sea ice (Hayashida et al., 2017), the monthly averaged amount is still expected to be lower than in productive open-ocean regions.

The modeled sea-to-air DMS emissions north of 60°N range from 0.20 to 0.26 Tg S yr^{-1}, which agrees well with the satellite-based estimate of 0.24 Tg S yr^{-1} over 2003–2016 (Gal et al., 2019). Note, however, that the satellite-based estimate lacks emissions from waters with more than 10% sea ice cover. On the other hand, the modeled emissions are lower than the estimate based on the L11 climatology (0.3 Tg S yr^{-1}; Lana et al., 2011). While there are a few differences between this study and Lana et al. (2011) in how the flux is calculated, the model simulates lower values primarily because of lower sea surface DMS concentration (Figure 1j).

3.2. Bottom Ice DMS Concentration

The evaluation of modeled DMS concentration within sea ice is challenging due to the scarcity of in situ measurements and the absence of other direct or indirect measurement techniques. Given the potential importance of sea ice DMS as a source of aerosols and cloud condensation nuclei (CCNs) in the Arctic during spring and summer, we discuss the timing and magnitude of annual maxima in modeled bottom ice DMS concentration (Figures 3a and 3b) and evaluate the findings via comparison with the small number of observed values reported in Levasseur (2013). Additionally, we compare the modeled time series in the Amundsen Gulf with the observed C13 data set.

3.2.1. Timing and Magnitude of Annual Maxima

The model simulates a peak month for bottom ice DMS concentration of May for most regions, while it is earlier (March or April) in the seasonal ice zone in lower latitudes and later (August) in the thick ice region north of Greenland and the Canadian Arctic Archipelago (Figure 3a). The seasonal ice zone is defined here as the area where sea ice is present seasonally. The spatial pattern of the peak concentration shows a shelf basin contrast similar to modeled ice algal biomass distribution (Watanabe et al., 2019); the peak concentration range is 100–1,000 μmol S m^{-3} in shelf regions, while its range is much lower (1–10 μmol m^{-3}) in the basins. There are only a few measurements of DMS within Arctic sea ice reported in Levasseur (2013): 30 μmol S m^{-3} in the Central Arctic in August 1994, 769 μmol S m^{-3} in the Beaufort Sea (year unknown), and 2,000 μmol S m^{-3} in the Resolute Bay in June 2012. While these measurements are instantaneous and therefore are not directly comparable to the (climatological) peak model concentration in this study, the values fall within the same order of magnitude for each of these measurement sites.

We note that the timing of annual maxima can be different from year to year. For example, the peak month in the Amundsen Gulf is May based on modeled climatological mean annual maxima (Figure 3a), whereas the analysis of individual years demonstrates that it can take place in April (Figure 3c).

3.2.2. Spatiotemporal Variability in the Amundsen Gulf

Figure 3c shows the time series of modeled and observed bottom ice DMS concentration between November 2007 and June 2008 in the Amundsen Gulf region defined in Figure 3a. Note that the model results are representative of monthly and regional averages, whereas the observed values are representative of in situ measurements at 23 different locations within the defined region. Hence, direct model-observation comparison is confounded by the difference in the spatial and temporal scales. To account for this uncertainty, we also show the minimum and maximum ranges in the modeled monthly mean values within the region.

Both the model and the observations show negligible concentration of bottom ice DMS from November to February. In March, the modeled mean and observed values are still low (50 μmol S m^{-3}), but the spatial variability increases in the model results as indicated by the spatial maximum of 400 μmol S m^{-3}. In April, the

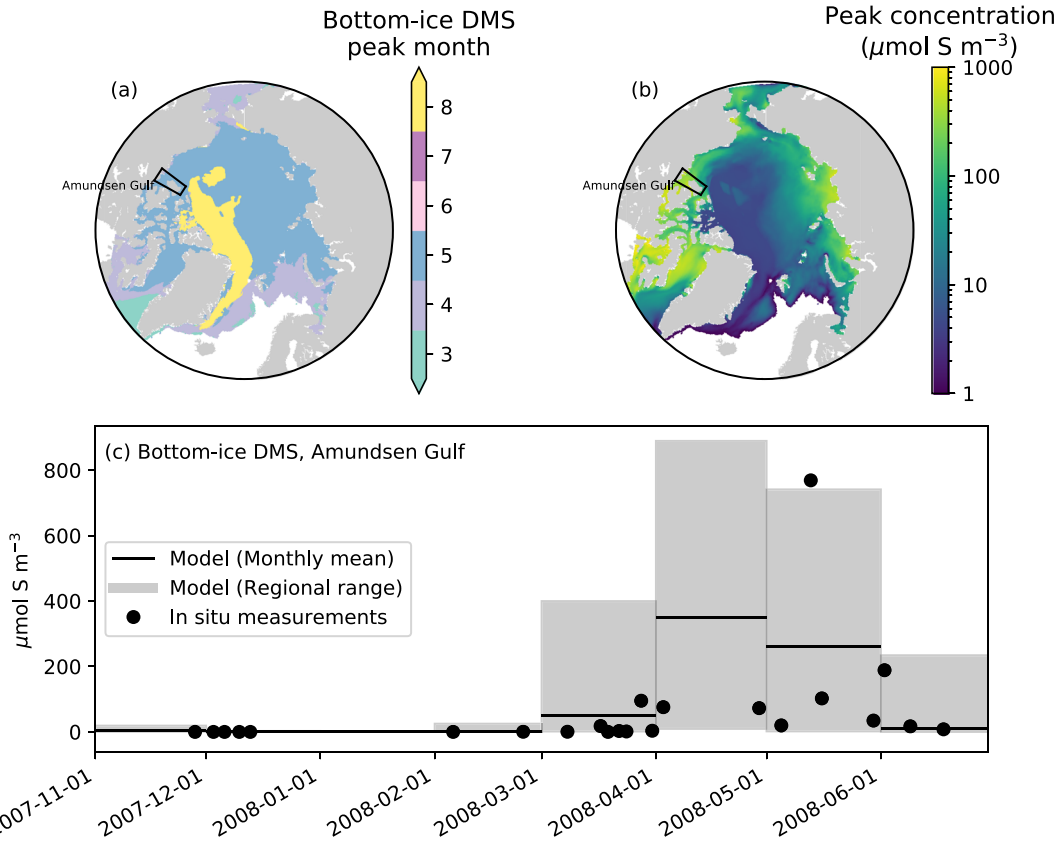

Figure 3. Modeled 1979–2015 climatological peak (a) month and (b) concentration of bottom ice DMS. (c) Time series comparison of bottom ice DMS concentration between in situ measurements (dots) and the model (lines) in the Amundsen Gulf. In subplots a and b, white colors represent areas either where the sea ice is absent or where the peak bottom ice DMS concentration is less than 1 μmol S m^{-3}. In subplot c, black lines denote monthly mean values averaged over the region bounded by black lines in subplots a and b (69–75°N and 119–127°W), and the lower and upper bounds of corresponding gray bars represent the monthly mean regional minimum and maximum, respectively.

modeled concentration is at its annual peak (with a mean concentration of approximately 350 μmol S m^{-3}) with values that can reach up to near 900 μmol S m^{-3} in the region. This peak in April cannot be verified by the observations due to the temporal gap in the sampling (only two data points for April). The observed maximum of 769 μmol S m^{-3} was sampled in mid-May and is associated with high ice algal biomass (655 mg *Chl* m^{-3}). This value is anomalously high compared to the other bottom ice DMS concentrations observed during this month and is near the maximum of monthly mean values simulated for this region. In June, both the modeled and observed values become negligible due to seasonal melting.

In summary, the model appropriately reflects the timing of the increase in DMS concentrations and shows elevated monthly and regional mean values during April and May with large spatial variability. Due to the small number of observations available for these months (six samples in total) and the large variability of DMS concentrations in space and time, these values need to be interpreted with caution. While the observed April mean is clearly lower than the model (74 vs. 349 μmol m^{-3}), the two values agree very well for May (232 vs. 262 μmol m^{-3}). Both model and observations demonstrate large spatial variability in bottom ice DMS concentration. This is not surprising particularly for these months, when observations are logistically extremely challenging and the light availability to ice algae is very patchy due to patchy snow distribution. This finding is consistent with a previous model study that shows even much higher peak concentrations in the region (about 3,000 μmol m^{-3} in May of 1992; Figure 2 of Elliott et al., 2012, after converting the concentration in the 10 m ocean product layer to that equivalent of the bottom 3 cm of sea ice).

3.3. Sea Surface DMS Concentration

FigureS 4a–4d show the modeled climatological monthly mean sea surface DMS concentration fields during May–August. Relatively high concentrations are simulated in open water areas of the Atlantic sector

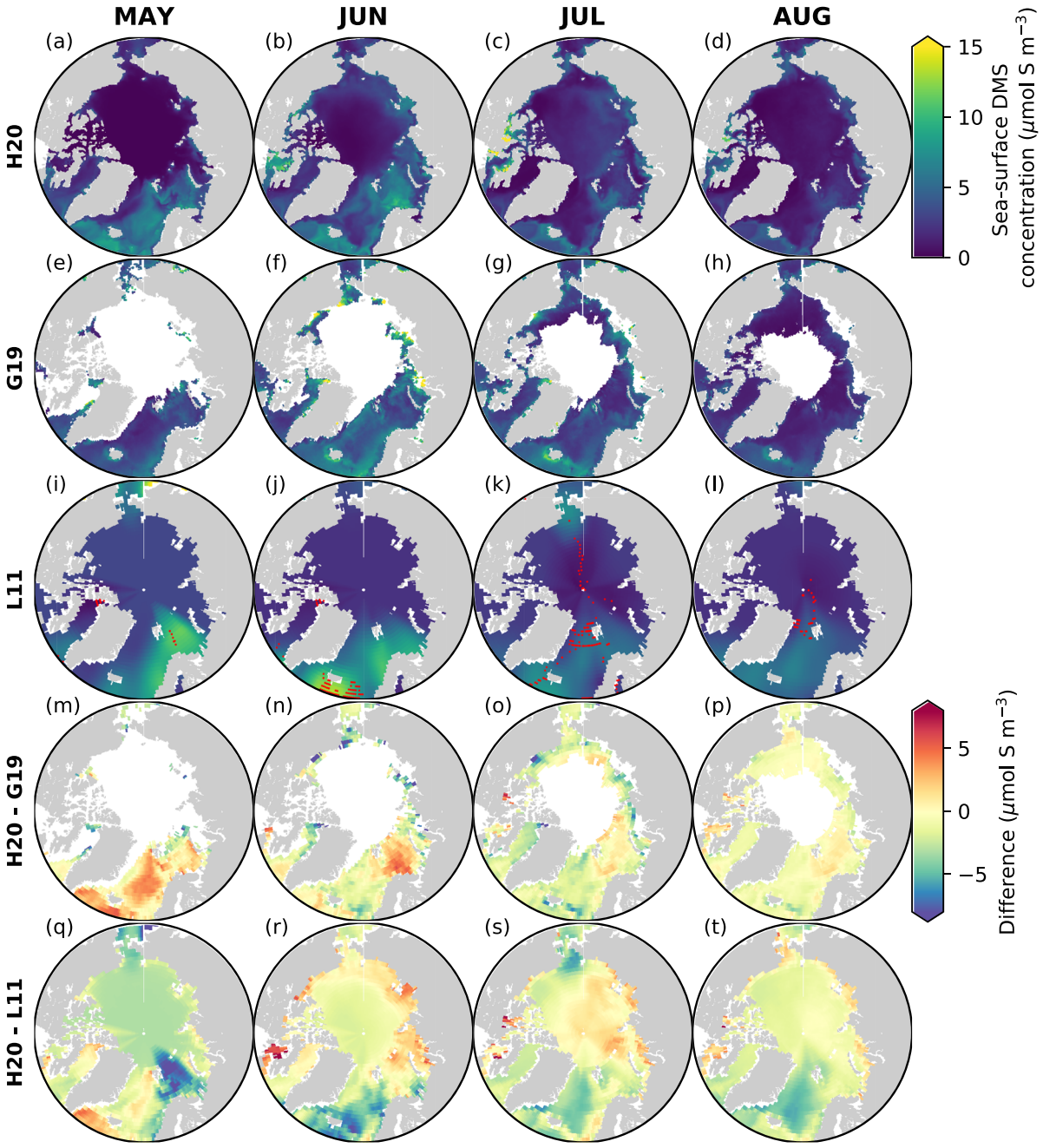

Figure 4. Spatial comparison of climatological monthly mean sea surface DMS concentration fields based on (a–d) model simulation over 1979–2015 (H20), (e–h) satellite observations over 2003–2016 (G19), and (i–l) the extrapolation of gridded in situ measurements indicated by red dots (L11). (m–p) The difference between the model- and satellite-based climatologies. (q–t) The difference between the model- and in situ measurement-based climatologies. White regions in subplots e–h either have no values due to the presence of sea ice or are masked due to signal contamination by riverine CDM. White regions in subplots m–t have no values due to the lack of data in either or both of the climatology data products.

with fine spatial details that are related to circulation patterns. Concentrations under the ice in the Central Arctic are near zero in May, slightly increase in June, and peak at about 4 μmol m^{-3} in July. The seasonal progression of DMS production in the region is driven by the underice phytoplankton bloom (Figures S7 and S8). The very high concentration (>14 μmol m^{-3}) in the Southern Canadian Polar Shelf is probably an artifact due to inadequate representation of the flow through fine channels in the region, resulting in an accumulation of nutrients and subsequent enhanced production (Figure S9).

Table 1
Statistics of Sea Surface DMS Concentration Comparisons Among the Model- (H20), Satellite- (G19), and In Situ Measurement-Based (L11) Climatology Products Over the Open Water Areas of the Pan-Arctic Domain Where the Data Exist for All of the Three Climatology Products After Interpolating to the 1° Grid of L11

	May	June	July	August
	Number of data points			
	1,177	1,671	2,315	2,695
	Mean ± spatial standard deviation (μmol m^{-3})			
H20	4.7 ± 1.9	4.3 ± 1.9	2.3 ± 1.5	1.6 ± 1.2
G19	3.5 ± 1.3	5.0 ± 2.0	3.7 ± 1.7	2.1 ± 1.2
L11	6.6 ± 2.8	6.1 ± 3.2	4.1 ± 1.7	3.6 ± 1.6
	Root-mean-square difference (μmol m^{-3})			
H20 versus G19	2.5	2.6	2.1	1.0
H20 versus L11	3.7	3.3	2.6	2.5
G19 versus L11	4.2	3.8	2.0	2.1
	Pearson's correlation coefficient (—)			
H20 versus G19	0.55	0.47	0.70	0.85
H20 versus L11	0.47	0.74	0.59	0.65
G19 versus L11	0.54	0.50	0.70	0.75

Note. Values are rounded to one decimal place for the mean, spatial standard deviation, and the root-mean-square difference and to two decimal places for the Pearson's correlation coefficient. In all cases, the *p* values associated with the correlation coefficients are below 0.05.

3.3.1. Comparison With the Satellite-Based Climatology

Figures 4e–4h show the satellite-based G19 DMS climatology. Note that the temporal coverage of the data used to construct the G19 climatology is 2003–2016, whereas the model-based climatology is based on 1979–2015. However, our preliminary analysis indicates that neither shortening the temporal coverage for the model-based climatology (e.g., 2003–2015; Figure S10) nor extending the satellite coverage (by incorporating data from the Sea-viewing Wide Field-of-view Sensor) qualitatively changes the outcome of the comparison. Also, it should be noted that satellite DMS values are representative of open water (where ice concentration is less than 10%), whereas the model incorporates both open water and ice-covered DMS values into the climatology. In satellite estimates, no value is assigned for a grid cell when ice concentration is 10% or greater. Consequently, some values in the satellite-based climatology are not representative of a stationary climate but are rather representative of a few years of satellite observations due to the ongoing reduction of sea ice cover in recent years. The G19 climatology shows relatively high concentration in the Atlantic sector (the Barents and Norwegian seas) and the northern Baffin Bay (North Water Polynya) in May. In June, high concentrations extend to the Greenland and Kara seas and to the seasonal ice zone on Arctic continental shelves. Concentrations decrease through July and August and do not feature high DMS along the ice margin.

Figures 4m–4p show the difference between the model- and satellite-based climatology fields over open water areas, where the modeled and satellite-derived monthly mean ice concentration values are both less than 10% at least once over their climatological periods. The model-based climatology is about 5 μmol m^{-3} higher in most of the Atlantic sector in May as well as in the Barents Sea in June. In contrast, the model-based climatology is about 5 μmol m^{-3} lower in the Beaufort, Chukchi, Laptev, and Kara shelf regions during June–July. The difference is relatively small in August, when both climatologies generally show relatively low DMS concentrations. Some frontal structures and circulation features present in the satellite-based climatology are well captured by the model, especially in the Atlantic sector, whereas poorer agreement is found in the seasonal ice zone over continental shelves. In particular, the relatively high value in the model-based climatology during July is driven by elevated DMS under the ice (Figure S7), which is by definition absent in the satellite-based climatology. The model-satellite difference in DMS is similar to that of chlorophyll *a* (Figure S11). The exception is when satellite chlorophyll *a* concentration is high (e.g., above

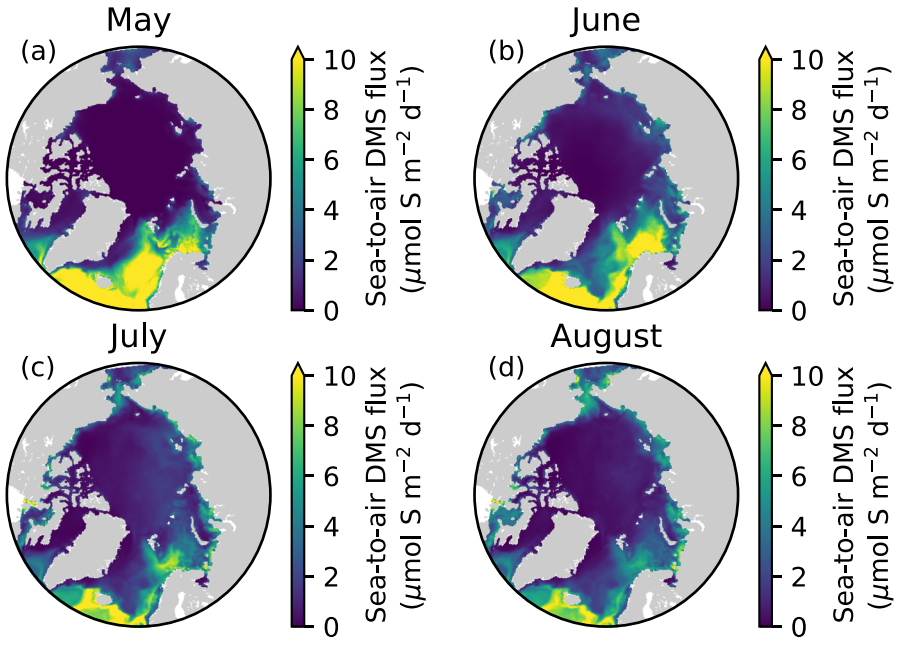

Figure 5. Pan-Arctic distribution of modeled climatological sea-to-air DMS flux in (a) May, (b) June, (c) July, and (d) August. Values represent monthly averages over 1979–2015.

5 mg m^{-3}). In this case, the corresponding satellite DMS concentration does not increase proportionally, resulting in closer agreement between the two products.

3.3.2. Comparison With the In Situ Measurement-Based Climatology

Figures 4i–4l show the in situ measurement-based L11 DMS climatology. The spatial-temporal coverage of gridded in situ measurements incorporated into this climatology is extremely limited for the Arctic domain. Specifically, these measurements are restricted to the northern Baffin Bay and the Barents Sea for May, the northern Baffin Bay and the northern North Atlantic for June, and the Fram Strait and the North Pole for August. The coverage for July is relatively large, including the northern North Atlantic, the Fram Strait, and the transpolar transect from the north of Svalbard to the northern Chukchi Sea.

In May, the L11 climatology shows relatively high concentration (>10 μmol m^{-3}) in the Norwegian Sea, the Barents Sea, and the western Bering Sea. In June, concentrations are still high in the Norwegian and Barents Seas as well as in the North Atlantic Ocean south of Iceland. In July and August, concentrations decrease in these regions (Figures 4k and 4l), while they increase in the Chukchi Sea in July. Unlike the model-based climatology, concentrations in the Central Arctic decrease from May to July. Contributing factors to the seasonal progression depicted by the L11 climatology in the region include the extrapolation of higher values from lower latitudes in May and the incorporation of local measurements of lower values in July.

Figures 4q–4t show the difference between the model- and in situ measurement-based climatology fields. The model generally simulates lower DMS concentrations in open water areas of the Atlantic and Pacific sectors except for regions south and southeast of Greenland in May. In contrast, the model simulates higher values in seasonally ice-covered shelf regions throughout June–August as well as in the Central Arctic during July. This discrepancy highlights the contribution of DMS production under the ice incorporated into the model-based climatology.

3.3.3. Statistical Comparison of Climatologies

Table 1 displays the statistical comparison of the three climatology products over the open water areas of the Pan-Arctic domain for which values are available from all three products. The model-based climatology is quantitatively closer to the satellite-based climatology than the in situ measurement-based climatology for all months, as indicated by the root-mean-square difference. The mean values of the L11 climatology are consistently higher than the other two products, especially in May and June. Again, these findings highlight the likely impacts of the extrapolation bias in the L11 climatology. However, we cannot rule out the possibility that negative biases occur in both the satellite and the model DMS fields, especially in areas where the

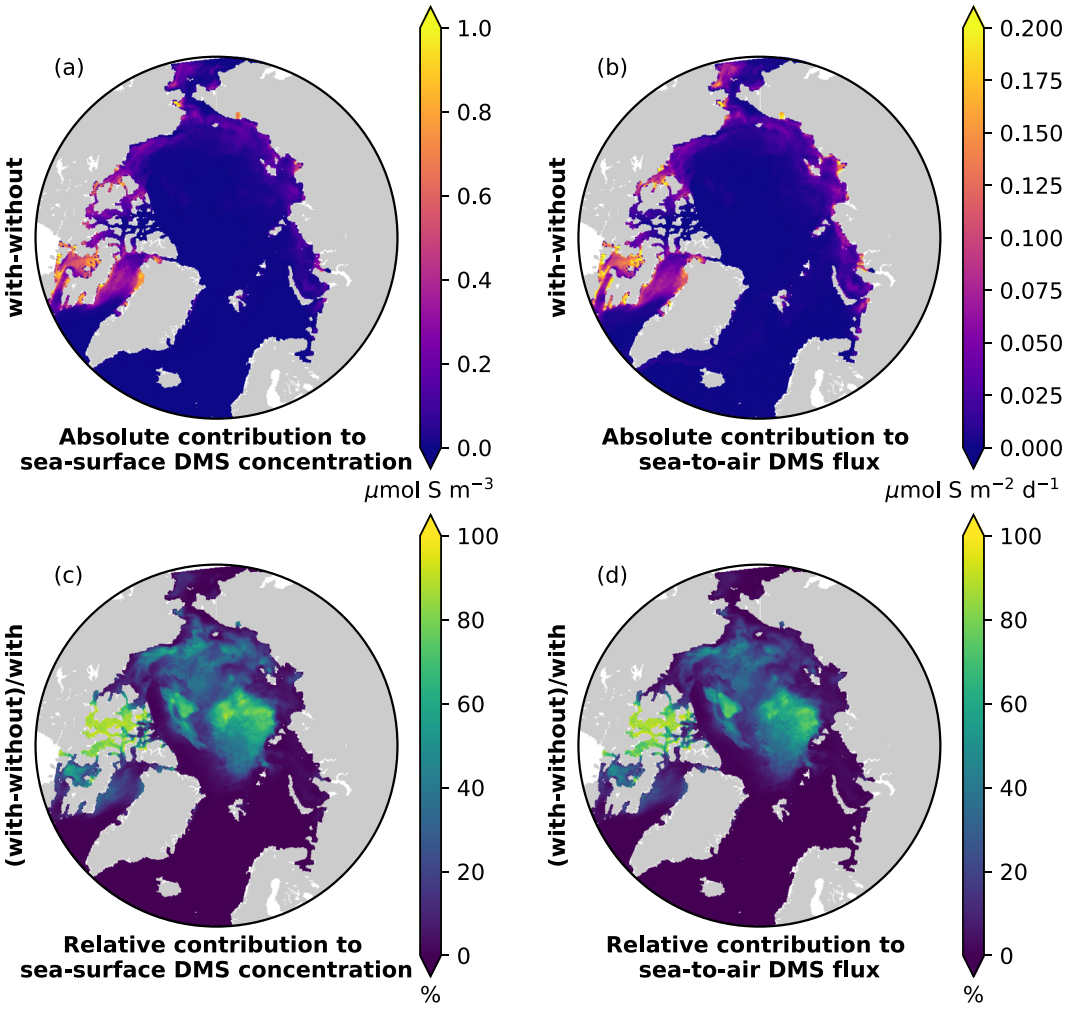

Figure 6. May mean contributions of modeled bottom ice DMSP and DMS production to sea surface DMS concentration and sea-to-air DMS flux averaged over 2006–2015. (a, b) Absolute contributions, as depicted by the concentration and flux differences between the model simulations with and without the representation of bottom ice DMSP and DMS production. (c, d) Relative contributions, as depicted by the with-minus-without differences divided by the simulated concentration and flux with the representation of bottom ice DMSP and DMS production.

L11 climatology suffers less from the extrapolation bias. The three products agree reasonably well in terms of spatial distribution for all months, as indicated by correlation coefficients of 0.47 or above in all cases.

To minimize the extrapolation bias in the L11 climatology, we compare the three climatology products that are subsampled over the open water grid cells that have in situ measurements prior (Figure S12). The results indicate that the model simulates less variability in sea surface DMS concentrations than the L11 climatology, but their median values are only 2 μmol m^{-3} apart. Similarly, we find that the model simulates less variability in DMS-to-chlorophyll *a* ratios than the observations, but they agree well in terms of the medians (Figure S13). These findings suggest that the model is skilful in simulating the broad spatial feature of DMS dynamics, while it lacks observed variability beyond the median. The satellite-based climatology is skilful in reproducing the observed variability including both the medians and the extremes.

3.4. Sea-to-Air DMS Flux

Figure 5 shows the modeled climatological monthly mean sea-to-air DMS flux fields. The spatial variability ranges from nearly zero flux in perennially ice-covered areas to fluxes exceeding 10 μmol m^{-2} day^{-1} in ice-free areas of the Atlantic sector. Fluxes between these lower and upper ends of the range take place in seasonally ice-covered shelf areas during June–August.

3.5. Simulation Without Bottom Ice DMSP and DMS Production

Figure 6 shows the contributions of modeled bottom ice DMSP and DMS production to sea surface DMS concentration and sea-to-air DMS flux during May, which is the month of highest bottom ice DMS concentration and ice-to-sea DMS flux over the pan-Arctic domain (Figures 1i and 1k). We consider both absolute and relative contributions to assess the overall impacts of the bottom ice production. The spatial patterns of the absolute contributions (Figures 6a and 6b) are similar to that of the annual bottom ice DMS concentration maxima (Figure 3b). Bottom ice DMSP and DMS production can supply more than 1 μmol m^{-3} of sea surface DMS concentration and 0.2 μmol m^{-2} day^{-1} of sea-to-air DMS flux in many parts of the Canadian Polar Shelf. Because of seasonal ice cover at this time of the year, DMS production by pelagic microbes is relatively low. As a result, the bottom ice production is responsible for the majority of DMS present in surface waters and consequently its flux into the atmosphere in the region, as indicated by high percentages in the relative contributions (Figures 3c and 3d). Furthermore, the bottom ice production is the sole source of sea surface DMS concentration and sea-to-air DMS flux in some of the region. Besides the Canadian Polar Shelf, a few locations along the coasts of Alaska and Russia experience similarly high levels of bottom ice contributions in both absolute and relative quantities.

We note a few cases where the bottom ice contributions can be high in absolute values but low in relative values, and vice versa. Under these circumstances, the overall impacts are deemed low. The first case is the combination of low-absolute and high-relative contributions as seen in many parts of the Central Arctic. Despite the low absolute contributions, the high relative contributions arise from extremely low values in the denominator in the percentage calculation. In contrast, high-absolute and low-relative contributions are the case for the Canadian Polar Shelf in June (Figure S14). In this case, despite the high absolute contributions, the bottom ice contributions are not as important as is in May due to an increase in DMS production in surface waters as a result of pelagic blooms (Figure 1h).

4. Discussion

In this study, we show that the accelerated decline of Arctic sea ice extent observed since the beginning of the 21st century is associated with contrasting responses of modeled ice-to-sea and sea-to-air fluxes of DMS over the pan-Arctic domain. Specifically, the ice-to-sea DMS flux exhibits strong interannual variability with no evident trend, whereas the sea-to-air DMS flux shows a quasi-linear upward trend. We also compare the spatiotemporal variability in the sea surface DMS climatology products based on three different approaches. Lastly, we quantify the contributions of the ice-to-sea flux of DMS and DMSP to the seasonal spatial structures of the sea surface DMS concentration and sea-to-air DMS flux for the first time at the pan-Arctic scale.

Satellite observations reveal a continuous decrease in the September Arctic sea ice extent since 1979 with an accelerated reduction since around the year 2000 (Stroeve et al., 2012). Using a model simulation assimilating observations, Schweiger et al. (2011) showed that the decrease in the extent was accompanied by a decrease in ice volume, which indicates that the Arctic sea ice is not only shrinking horizontally but is also thinning vertically. The horizontal shrinking and the vertical thinning of sea ice have counteracting effects on ice algal production, resulting in no apparent trend in the modeled ice-to-sea DMS flux. In contrast, the accelerated decline of Arctic sea ice extent is associated with an upward trend in open water primary production over the pan-Arctic domain as previously suggested by satellite observations (Arrigo & van Dijken, 2015). Our model results, which include contributions from ice-covered areas, exhibit a general increase in sea surface primary production and an increase in sea surface DMS concentration. Consequently, the changes in sea ice increase the modeled sea-to-air DMS flux due to both direct (more emission due to increased open water areas) and indirect (more production due to increased light availability) effects.

Global climate and Earth system models project that Arctic sea ice will continue to decline throughout the 21st century with a greater likelihood of seasonal ice-free conditions by the middle century (Stroeve & Notz, 2018; Thackeray & Hall, 2019). Although our results may suggest a continued increase in oceanic DMS emissions throughout this century, the longer-term response in the coming decades may be different due to an anticipated increase in nutrient stress (Steiner et al., 2015; Vancoppenolle et al., 2013). Nutrient stress has counteracting effects on DMS production; it can decrease production by limiting photosynthetic growth, while it can promote production by increasing the intracellular DMSP-to-carbon ratios of algal species (especially diatoms McParland & Levine, 2019). Furthermore, the response will also depend on potential changes

in ecological processes that are induced by climate change. Recent studies have already observed such changes including poleward expansion of Emiliania huxleyi in the Barents Sea (Neukermans et al., 2018) and potential increase in the abundance of Phaeocystis pouchetii in the Fram Strait (Nöthig et al., 2015; Soltwedel et al., 2016) that are known as high DMSP producers (Stefels et al., 2007). Although these species are included as small phytoplankton in our model, having an explicit representation of individual species would allow more detailed assessment of their role in oceanic DMS production (Wang et al., 2015). While a model that incorporates these species may help better understand the overall impacts of Arctic warming on DMS production and emissions, the computational requirements associated with additional phytoplankton groups are a limiting factor. Another difficulty is that including more species in models requires the introduction of more parameters and parameterized interactions pertaining to specific species as well as ecological interactions among multiple species. Such increases in model complexity require substantial increases in the number and diversity of observations so that the model is properly constrained. Such an effort is a valuable direction for future study but at the same time requires careful consideration because it introduces an additional source of uncertainty without necessarily leading to better results (Matear, 1995).

The representation of oceanic DMS emissions in many global climate and Earth system models relies on the in situ measurement-based climatological sea surface DMS concentration fields that are based on extremely limited data coverage over the Arctic domain. Given these limited observations, the evaluation of the model- and satellite-based Arctic DMS climatology products is challenging. Our results indicate higher spatial variability in these products than the in situ measurement-based climatology. The claim for higher variability is supported by the data collected from recent field campaigns (Abbatt et al., 2019; Jarnkov et al., 2018; Lizotte et al., 2020). These data can improve the quality of the Arctic DMS climatology by increasing the data coverage, as these field campaigns focused on regions lacking data in the L11 climatology, such as the Canadian Polar Shelf during July–August. Furthermore, the interannual variability and trends in sea surface DMS concentration fields in the Arctic can be nontrivial (e.g., 19% increase in the pan-Arctic mean sea surface DMS concentration over 2001–2015 based on our model results) and therefore can represent an important source of interannual variability and trends in sulfate aerosol and cloud formation processes in the Arctic (Gal et al., 2019).

Previous studies have suggested the potential importance of DMSP and DMS produced within sea ice to oceanic DMS emissions (Elliott et al., 2012; Hayashida et al., 2017; Levasseur et al., 1994). Although ice algae blooms are often dominated by diatoms which are generally low DMSP producers in extrapolar environments (Stefels et al., 2007), the cellular content of DMSP relative to biomass for bottom ice diatoms is found to be about 4 times more than that of pelagic diatoms in lower latitudes (see Appendix A; Galindo et al., 2014; Stefels et al., 2007), likely due to the use of DMSP as cryoprotectant (Kirst et al., 1991). In addition, the biomass of ice algae can be large enough to generate comparable amounts of DMSP and DMS as high DMSP producers. Another important aspect of diatoms is that nutrient stress could amplify the cellular DMSP content, and hence the DMS production, by an order of magnitude, as suggested by the global study of McParland and Levine (2019). Our model results suggest that bottom ice DMSP and DMS produced by diatoms can make a substantial contribution to the sea surface DMS concentration and sea-to-air flux fields at the beginning of melting season prior to pelagic blooms and in regions where bottom ice DMS production is high. This contribution can be crucial for the new particle formation in the Arctic due to the low background concentration of CCNs at that time of the year (Sharma et al., 2012). Empirical assessment of the model-based finding with more in situ measurements is desirable but is not possible in the present study due to limited observations. Such a determination can be achieved by undertaking field observations targeting bottom ice and sea surface DMS concentrations in the Canadian Arctic in late spring.

It should be acknowledged that our results more likely underestimate than overestimate the contribution of bottom ice DMSP and DMS due to simplifications in the model. Specifically, our model does not account for processes such as intracellular and membrane-bound algal DMSP-lyase activities, dimethylsulfoxide reduction, brine drainage, and bubble formation, all of which would increase the production and release of bottom ice DMSP and DMS (Hayashida et al., 2017). A recent field study has quantified for the first time the upward transport of DMS from the bottom ice to the atmosphere via diffusion and bubble formation (Gourdal et al., 2019). Further observational constraints such as those in Gourdal et al. (2019) are needed to incorporate these processes into models for improvements. In addition, better knowledge of the relationship between sea ice concentration and gas exchange is needed, as contradictory results are found in the literature (Loose et al., 2014; Rutgers van der Loeff et al., 2014). Lastly, field observations demonstrate that

melt ponds are an additional sea ice habitat for DMS production that add to oceanic DMS emissions in ice-covered regions during summer (Gourdal et al., 2018; Levasseur, 2013; Park et al., 2019). Although a previous study has suggested that melt pond DMS flux can temporarily be the sole source of atmospheric DMS in ice-covered regions (Mungall et al., 2016), further studies are needed to develop a mechanistic understanding of DMS production within melt ponds and its release into the atmosphere. Pursuing such research is an interesting future direction of collaboration between modelers and observationalists.

5. Summary and Conclusions

Using a regional sea ice-ocean physical-biogeochemical model, we investigated the spatiotemporal variability in bottom ice and sea surface DMS concentrations and fluxes in the Arctic during 1979–2015. A summary of key findings and conclusions is provided below.

- The model successfully simulates the observed accelerated decline of Arctic sea ice since the beginning of the 21st century.
- The decline of Arctic sea ice is associated with strong interannual variability with no evident trends in the modeled bottom ice algal biomass, bottom ice DMS concentration, and ice-to-sea DMS flux averaged over the pan-Arctic (north of 60°N). These temporal variations are reasonable given that the horizontal shrinking and vertical thinning of sea ice have counteracting effects on ice algal production.
- In contrast to the bottom ice biogeochemical properties, the sea ice decline promotes primary production in seawater due to increased light availability for photosynthesis and therefore is associated with quasi-linear upward trends in the pan-Arctic mean sea surface phytoplankton biomass (14% increase in May–August averages over 2001–2015), sea surface DMS concentration (19%), and sea-to-air DMS flux (39%).
- The model- and satellite-based Arctic DMS climatologies exhibit dynamically based spatial details that are absent in the in situ measurement-based climatology due to extremely sparse data coverage and consequent strong extrapolation from subpolar regions, which might have implications for the spatial and temporal variability of sulfate aerosol and clouds over the Arctic.
- The bottom ice DMSP and DMS production can be the sole source of DMS present in and released from surface waters and therefore make substantial contributions to sea surface DMS concentration and sea-to-air DMS flux over extended regions in late spring prior to pelagic blooms.
- Ultimately, it is essential to develop climate models with prognostic sea ice and ocean biogeochemistry that accounts for the interannual and longer-term variability in oceanic DMS emissions in order to comprehensively address the biological control on Arctic climate.

Appendix A: DMSP and DMS Model Equations

Bottom ice DMSPp ($DMSPp_{bi}$) and seawater DMSPp ($DMSPp_{sw}$) concentrations are modeled diagnostically as the product of the intracellular DMSP-to-carbon ratio and the biomass of each algal group:

$$DMSPp_{bi} = q_{ia} IA \tag{A1}$$

$$DMSPp_{sw} = q_{p1} P1 + q_{p2} P2 \tag{A2}$$

where q_{ia}, q_{p1}, and q_{p2} are the intracellular ratios for ice algae (IA), small phytoplankton ($P1$), and large phytoplankton ($P2$), respectively. q_{ia} is set to 4 mmol S:mol C by converting the DMSP-to-chlorophyll a ratio for diatom-dominated ice algae in Resolute Passage (9.5 mmol S:g Chl Galindo et al., 2014) to the DMSP-to-carbon ratio by assuming a carbon-to-chlorophyll a ratio of 28 g C:g Chl (Lavoie et al., 2005). Although this assumption neglects the dependence of the ratio on light and nutrient availability (Geider et al., 1998), it is consistent with the method used to derive the DMSP-to-carbon ratios for major algal species (Stefels et al., 2007), in which the DMSP-to-carbon ratio is assumed 60 g C:g Chl, typical for cultures that grow under light replete and nutrient replete conditions (Geider, 1987). q_{p1} is set to 12 mmol S:mol C, representative of high DMSP producer haptophytes (Stefels et al., 2007). In contrast, q_{p2} is set to 4 mmol S:mol C, representative of diatoms. This value is equivalent to q_{ia}, as ice algae enter the large phytoplankton pool when they are released from the bottom ice. This value is reasonable given the observed range of 2.5–5.3 mmol S:mol C for underice diatom-dominated phytoplankton in Resolute Passage (after applying the conversion factor of 28 g C:g Chl Galindo et al., 2014).

Bottom ice DMSPd ($DMSPd_{bi}$) and seawater DMSPd ($DMSPd_{sw}$) concentrations are modeled prognostically:

$$\frac{\partial}{\partial t}(DMSPd_{bi}) = F^{bi}_{lysis} + F^{bi}_{exudation} - F^{dmspd_{bi}}_{consumption} - F^{bi}_{free} - \frac{F^{dmsp}_{ice-to-sea}}{h_{bi}} \quad \text{(A3)}$$

$$\frac{\partial}{\partial t}(DMSPd_{sw}) = F^{sw}_{lysis} + F^{sw}_{exudation} + F^{sw}_{sloppy} - F^{dmspd_{sw}}_{consumption} - F^{sw}_{free} + \frac{F^{dmsp}_{ice-to-sea}}{h_{z0}}\delta_{z,z0} \quad \text{(A4)}$$

In these equations, DMSPd is produced by cell lysis (F^{bi}_{lysis}, F^{sw}_{lysis}), exudation ($F^{bi}_{exudation}$, $F^{sw}_{exudation}$), and sloppy feeding (F^{sw}_{sloppy}; seawater only), whereas it is removed by bacterial consumption and free-lyase activity. DMSPd is released from the bottom ice to the surface ocean by ice-to-sea flux ($F^{DMSPd}_{ice-to-sea}$). h_{bi} and $_{z0}$ denote the vertical thickness of the bottom ice skeletal layer (0.03 m) and the uppermost ocean layer (approximately 1 m), respectively. Kronecker's delta ($\delta_{z,z0}$) equals one at the uppermost ocean layer ($z0$), whereas it is zero elsewhere.

Bottom ice DMS (DMS_{bi}) and seawater DMS (DMS_{sw}) concentrations are modeled prognostically:

$$\frac{\partial}{\partial t}(DMS_{bi}) = F^{bi}_{conversion} + F^{bi}_{free} - F^{dms_{bi}}_{consumption} - F_{photo} - \frac{F^{dms}_{ice-to-sea}}{h_{bi}} \quad \text{(A5)}$$

$$\frac{\partial}{\partial t}(DMS_{sw}) = F^{sw}_{conversion} + F^{sw}_{free} - F^{dms_{sw}}_{consumption} - F^{sw}_{photo} - \frac{F^{dms}_{ice-to-sea}}{h_{z0}}\delta_{z,z0} - \frac{F_{sea-to-air}}{h_{z0}}\delta_{z,z0} \quad \text{(A6)}$$

In these equations, DMS is produced by bacterial conversion ($F^{bi}_{conversion}$, $F^{sw}_{conversion}$) and free-lyase activity, whereas it is removed by bacterial consumption ($F^{dms_{bi}}_{consumption}$, $F^{dms_{sw}}_{consumption}$) and photolysis ($F^{bi}_{photo}$, F^{sw}_{photo}). DMS is released from the bottom ice to the surface ocean by ice-to-sea flux ($F^{dms}_{ice-to-sea}$) and from the surface ocean to the atmosphere by sea-to-air flux ($F_{sea-to-air}$).

The terms on the right-hand side of Equations A3–A6 are described in supporting information.

Data Availability Statement

The satellite data sets were provided by the Takuvik Joint UL/CNRS Laboratory team. The model code and output supporting the key findings of the present study are available online (https://doi.org/10.5281/zenodo.3697356). The satellite-based DMS climatology is available online (https://doi.org/10.5281/zenodo.3243967). PHC3.0 is available at https://psc.apl.washington.edu/nonwp_projects/PHC/Climatology.html website. ORAS4 is available at https://icdc.cen.uni-hamburg.de/projekte/easy-init/easy-init-ocean.html website. DFS5.2 is available at https://www.drakkar-ocean.eu/ website. The Sea Ice Index Version 3 is available online (https://nsidc.org/data/G02135/versions/3). The L11 climatology is available online (https://www.bodc.ac.uk/solas_integration/implementation_products/group1/dms/). The sea ice DMS profiles in the Amundsen Gulf can be made available upon request to G. C.

Acknowledgments
We thank James R. Christian for his helpful comments on an earlier version of this manuscript. The present study contributes to the SCOR Working group on Biogeochemical Exchange Processes at Sea Ice Interfaces (BEPSII), the Network on Climate and Aerosols: Addressing Key Uncertainties in Remote Canadian Environments (NETCARE), and ArcticNet. We acknowledge funding from NETCARE and ArcticNet. N. S. acknowledges support from Fisheries and Oceans and Environment and Climate Change Canada. T. S. acknowledges support through Fisheries and Oceans' Aquatic Climate Change Adaptation Services Program (ACCASP). This research was enabled in part by support provided by WestGrid and Compute Canada. We are grateful to Belaid Moa for computational support.

References

Abbatt, J. P. D., Leaitch, W. R., Aliabadi, A. A., Bertram, A. K., Blanchet, J.-P., Boivin-Rioux, A., et al. (2019). Overview paper: New insights into aerosol and climate in the Arctic. *Atmospheric Chemistry and Physics*, *19*(4), 2527–2560. https://doi.org/10.5194/acp-19-2527-2019

Andreae, M. O., & Crutzen, P. J. (1997). Atmospheric aerosols: Biogeochemical sources and role in atmospheric chemistry. *Science*, *276*(5315), 1052–1058. https://doi.org/10.1126/science.276.5315.1052

Arrigo, K. R., & van Dijken, G. L. (2015). Continued increases in Arctic Ocean primary production. *Progress in Oceanography*, *136*, 60–70. https://doi.org/10.1016/j.pocean.2015.05.002

Aumont, O., Ethé, C., Tagliabue, A., Bopp, L., & Gehlen, M. (2015). PISCES-v2: An ocean biogeochemical model for carbon and ecosystem studies. *Geoscientific Model Development*, *8*(8), 2465–2513. https://doi.org/10.5194/gmd-8-2465-2015

Aumont, O., Maier-Reimer, E., Blain, S., & Monfray, P. (2003). An ecosystem model of the global ocean including Fe, Si, P colimitations. *Global Biogeochemical Cycles*, *17*(2), 1060. https://doi.org/10.1029/2001GB001745

Balmaseda, M. A., Mogensen, K., & Weaver, A. T. (2013). Evaluation of the ECMWF ocean reanalysis system ORAS4. *Quarterly Journal of the Royal Meteorological Society*, *139*(674), 1132–1161. https://doi.org/10.1002/qj.2063

Bouillon, S., Maqueda, M. A. M., Legat, V., & Fichefet, T. (2009). An elasticviscousplastic sea ice model formulated on Arakawa B and C grids. *Ocean Modelling*, *27*(3), 174–184. https://doi.org/10.1002/qj.2063

Carnat, G. (2013). Towards an understanding of the physical and biological controls on the cycling of dimethylsulfide (DMS) in Arctic and Antarctic sea ice (Doctoral dissertation). http://mspace.lib.umanitoba.ca/xmlui/handle/1993/23732

Carnat, G., Papakyriakou, T., Geilfus, N. X., Brabant, F., Delille, B., Vancoppenolle, M., et al. (2013). Investigations on physical and textural properties of Arctic first-year sea ice in the Amundsen Gulf, Canada, November 2007 June 2008 (IPY-CFL system study). *Journal of Glaciology*, *59*(217), 819–837. https://doi.org/10.3189/2013JoG12J148

Chang, R. Y.-W., Sjostedt, S. J., Pierce, J. R., Papakyriakou, T. N., Scarratt, M. G., Michaud, S., et al. (2011). Relating atmospheric and oceanic DMS levels to particle nucleation events in the Canadian Arctic. *Journal of Geophysical Research*, *116*, D00S03. https://doi.org/10.1029/2011JD015926

Cleveland, W. S. (1979). Robust locally weighted regression and smoothing scatterplots. *Journal of the American Statistical Association*, *74*(368), 829–836. https://doi.org/10.1080/01621459.1979.10481038

Dussin, R., Barnier, B., Brodeau, L., & Molines, J. M. (2016). The making of the Drakkar forcing set DFS5. DRAKKAR/MyOcean Rep. 0104, 16.

Elliott, S., Deal, C., Humphries, G., Hunke, E., Jeffery, N., Jin, M., et al. (2012). Pan-Arctic simulation of coupled nutrient-sulfur cycling due to sea ice biology: Preliminary results. *Journal of Geophysical Research*, *117*, G01016. https://doi.org/10.1029/2011JG001649

Fetterer, F., Knowles, K., Meier, W., Savoie, M., & Windnagel, A. (2017). Sea ice index, version 3. Boulder, Colorado USA: National Snow and Ice Data Center (NSIDC). https://doi.org/10.7265/n5k072f8

Fichefet, T., & Maqueda, M. A. M. (1997). Sensitivity of a global sea ice model to the treatment of ice thermodynamics and dynamics. *Journal of Geophysical Research*, *102*(C6), 12,609–12,646. https://doi.org/10.1029/97JC00480

Gabric, A. J., Matrai, P. A., & Vernet, M. A. (1999). Modelling the production and cycling of dimethylsulphide during the vernal bloom in the Barents Sea. *Tellus B: Chemical and Physical Meteorology*, *51*(5), 919–937. https://doi.org/10.3402/tellusb.v51i5.16505

Gabric, A. J., Qu, B., Matrai, P., & Hirst, A. C. (2005). The simulated response of dimethylsulfide production in the Arctic Ocean to global warming. *Tellus B*, *57*(5), 391–403. https://doi.org/10.1111/j.1600-0889.2005.00163.x

Gal, M., Devred, E., Babin, M., & Levasseur, M. (2019). Decadal increase in Arctic dimethylsulfide emission. *Proceedings of the National Academy of Sciences*, *116*, 19,311–19,317. https://doi.org/10.1073/pnas.1904378116

Galindo, V., Levasseur, M., Mundy, C. J., Gosselin, M., Tremblay, J.-E., Scarratt, M., et al. (2014). Biological and physical processes influencing sea ice, under-ice algae, and dimethylsulfoniopropionate during spring in the Canadian Arctic Archipelago. *Journal of Geophysical Research: Oceans*, *119*, 3746–3766. https://doi.org/10.1002/2013JC009497

Geider, R. J. (1987). Light and temperature dependence of the carbon to chlorophyll a ratio in microalgae and cyanobacteria: Implications for physiology and growth of phytoplankton. *The New Phytologist*, *106*(1), 1–34. Publisher: [Wiley, New Phytologist Trust] https://www.jstor.org/stable/2434683

Geider, R. J., Maclntyre, H. L., & Kana, T. M. (1998). A dynamic regulatory model of phytoplanktonic acclimation to light, nutrients, and temperature. *Limnology and Oceanography*, *43*(4), 679–694. https://doi.org/10.4319/lo.1998.43.4.0679

Ghahremaninezhad, R., Norman, A.-L., Abbatt, J. P. D., Levasseur, M., & Thomas, J. L. (2016). Biogenic, anthropogenic and sea salt sulfate size-segregated aerosols in the Arctic summer. *Atmospheric Chemistry and Physics*, *16*(8), 5191–5202. https://doi.org/10.5194/acp-16-5191-2016

Gosselin, M., Legendre, L., Therriault, J.-C., & Demers, S. (1990). Light and nutrient limitation of sea-ice microalgae (Hudson Bay, Canadian Arctic). *Journal of Phycology*, *26*(2), 220–232. https://doi.org/10.1111/j.0022-3646.1990.00220.x

Gourdal, M., Crabeck, O., Lizotte, M., Galindo, V., Gosselin, M., Babin, M., et al. (2019). Upward transport of bottom-ice dimethyl sulfide during advanced melting of arctic first-year sea ice. *Elementa: Science of the Anthropocene*, *7*(1), 33. https://doi.org/10.1525/elementa.370

Gourdal, M., Lizotte, M., Massé, G., Gosselin, M., Poulin, M., Scarratt, M., et al. (2018). Dimethyl sulfide dynamics in first-year sea ice melt ponds in the Canadian Arctic Archipelago. *Biogeosciences*, *15*(10), 3169–3188. https://doi.org/10.5194/bg-15-3169-2018

Hayashida, H. (2018). Modelling sea-ice and oceanic dimethylsulfide production and emissions in the Arctic (PhD Thesis), Victoria, BC, Canada. https://dspace.library.uvic.ca//handle/1828/10486

Hayashida, H., Christian, J. R., Holdsworth, A. M., Hu, X., Monahan, A. H., Mortenson, E., et al. (2019). CSIB v1 (Canadian Sea-ice Biogeochemistry): A sea-ice biogeochemical model for the NEMO community ocean modelling framework. *Geoscientific Model Development*, *12*(5), 1965–1990. https://doi.org/10.5194/gmd-12-1965-2019

Hayashida, H., Steiner, N., Monahan, A., Galindo, V., Lizotte, M., & Levasseur, M. (2017). Implications of sea-ice biogeochemistry for oceanic production and emissions of dimethyl sulfide in the Arctic. *Biogeosciences*, *14*(12), 3129–3155. https://doi.org/10.5194/bg-14-3129-2017

Hu, X., & Myers, P. G. (2014). Changes to the Canadian Arctic archipelago sea ice and freshwater fluxes in the twenty-first century under the intergovernmental panel on climate change A1B climate scenario. *Atmosphere-Ocean*, *52*(4), 331–350. https://doi.org/10.1080/07055900.2014.942592

Humphries, G. R. W., Deal, C. J., Elliott, S., & Huettmann, F. (2012). Spatial predictions of sea surface dimethylsulfide concentrations in the high arctic. *Biogeochemistry*, *110*(1–3), 287–301. https://doi.org/10.1007/s10533-011-9683-y

Jarnkov, T., Dacey, J., Lizotte, M., Levasseur, M., & Tortell, P. (2018). The distribution of methylated sulfur compounds, DMS and DMSP, in Canadian subarctic and Arctic marine waters during summer 2015. *Biogeosciences*, *15*(8), 2449–2465. https://doi.org/10.5194/bg-15-2449-2018

Jodwalis, C. M., Benner, R. L., & Eslinger, D. L. (2000). Modeling of dimethyl sulfide ocean mixing, biological production, and sea-to-air flux for high latitudes. *Journal of Geophysical Research*, *105*(D11), 14,387–14,399. https://doi.org/10.1029/2000JD900023

Kettle, A. J., & Andreae, M. O. (2000). Flux of dimethylsulfide from the oceans: A comparison of updated data sets and flux models. *Journal of Geophysical Research*, *105*(D22), 26,793–26,808. https://doi.org/10.1029/2000JD900252

Kettle, A. J., Andreae, M. O., Amouroux, D., Andreae, T. W., Bates, T. S., Berresheim, H., et al. (1999). A global database of sea surface dimethylsulfide (DMS) measurements and a procedure to predict sea surface DMS as a function of latitude, longitude, and month. *Global Biogeochemical Cycles*, *13*(2), 399–444. https://doi.org/10.1029/1999GB900004

Kirst, G. O., Thiel, C., Wolff, H., Nothnagel, J., Wanzek, M., & Ulmke, R. (1991). Dimethylsulfoniopropionate (DMSP) in icealgae and its possible biological role. *Marine Chemistry*, *35*, 381–388. https://doi.org/10.1016/S0304-4203(09)90030-5

Lana, A., Bell, T. G., Simó, R., Vallina, S. M., Ballabrera-Poy, J., Kettle, A. J., et al. (2011). An updated climatology of surface dimethlysulfide concentrations and emission fluxes in the global ocean. *Global Biogeochemical Cycles*, *25*, GB1004. https://doi.org/10.1029/2010GB003850

Lauvset, S. K., Key, R. M., Olsen, A., van Heuven, S., Velo, A., Lin, X., et al. (2016). A new global interior ocean mapped climatology: The 1-deg. by 1-deg. GLODAP version 2. *Earth System Science Data*, *8*, 325–340. https://doi.org/10.5194/essd-8-325-2016

Lavoie, D., Denman, K., & Michel, C. (2005). Modeling ice algal growth and decline in a seasonally ice-covered region of the Arctic (Resolute Passage, Canadian Archipelago). *Journal of Geophysical Research*, *110*, C11009. https://doi.org/10.1029/2005JC002922

Lawrence, I. R., Tsamados, M. C., Stroeve, J. C., Armitage, T. W. K., & Ridout, A. L. (2018). Estimating snow depth over Arctic sea ice from calibrated dual-frequency radar freeboards. *The Cryosphere*, *12*(11), 3551–3564. https://doi.org/10.5194/tc-12-3551-2018

Levasseur, M. (2013). Impact of Arctic meltdown on the microbial cycling of sulphur. *Nature Geoscience*, *6*(9), 691–700. https://doi.org/10.1038/ngeo1910

Levasseur, M., Gosselin, M., & Michaud, S. (1994). A new source of dimethylsulfide (DMS) for the Arctic atmosphere: Ice diatoms. *Marine Biology*, *121*(2), 381–387. https://doi.org/10.1007/BF00346748

Lizotte, M., Levasseur, M., Galindo, V., Gourdal, M., Gosselin, M., Tremblay, J.-E., et al. (2020). Phytoplankton and dimethylsulfide dynamics at two contrasting Arctic ice edges. *Biogeosciences*, *17*(6), 1557–1581. Publisher: Copernicus GmbH https://doi.org/10.5194/bg-17-1557-2020

Loose, B., McGillis, W. R., Perovich, D., Zappa, C. J., & Schlosser, P. (2014). A parameter model of gas exchange for the seasonal sea ice zone. *Ocean Science*, *10*(1), 17–28. https://doi.org/10.5194/os-10-17-2014

Madec, G. (2008). NEMO ocean engine (Tech. Rep. No. 27). Institut Pierre Simon Laplace (ISPL).

Maritorena, S., Siegel, D. A., & Peterson, A. R. (2002). Optimization of a semianalytical ocean color model for global-scale applications. *Applied Optics*, *41*(15), 2705–2714. https://doi.org/10.1364/AO.41.002705

Matear, R. J. (1995). Parameter optimization and analysis of ecosystem models using simulated annealing: A case study at Station P. *Journal of Marine Research*, *53*(4), 571–607.

McParland, E. L., & Levine, N. M. (2019). The role of differential DMSP production and community composition in predicting variability of global surface DMSP concentrations. *Limnology and Oceanography*, *64*(2), 757–773. https://doi.org/10.1002/lno.11076

Meiners, K. M., Vancoppenolle, M., Carnat, G., Castellani, G., Delille, B., Delille, D., et al. (2018). Chlorophyll-a in Antarctic landfast sea ice: A first synthesis of historical ice core data. *Journal of Geophysical Research: Oceans*, *123*, 8444–8459. https://doi.org/10.1029/2018JC014245

Mortenson, E., Hayashida, H., Steiner, N., Monahan, A., Blais, M., Gale, M. A., et al. (2017). A model-based analysis of physical and biological controls on ice algal and pelagic primary production in Resolute Passage. *Elementa: Science of the Anthropocene*, *5*, 39. https://doi.org/10.1525/elementa.229

Mungall, E. L., Croft, B., Lizotte, M., Thomas, J. L., Murphy, J. G., Levasseur, M., et al. (2016). Dimethyl sulfide in the summertime Arctic atmosphere: Measurements and source sensitivity simulations. *Atmospheric Chemistry and Physics*, *16*(11), 6665–6680. https://doi.org/10.5194/acp-16-6665-2016

Neukermans, G., Oziel, L., & Babin, M. (2018). Increased intrusion of warming Atlantic water leads to rapid expansion of temperate phytoplankton in the Arctic. *Global Change Biology*, *24*(6), 2545–2553. https://doi.org/10.1111/gcb.14075

Nöthig, E.-M., Bracher, A., Engel, A., Metfies, K., Niehoff, B., Peeken, I., et al. (2015). Summertime plankton ecology in Fram Straita compilation of long- and short-term observations. *Polar Research*, *34*(1), 23349. https://doi.org/10.3402/polar.v34.23349

Park, K.-T., Jang, S., Lee, K., Yoon, Y. J., Kim, M.-S., Park, K., et al. (2017). Observational evidence for the formation of DMS-derived aerosols during Arctic phytoplankton blooms. *Atmospheric Chemistry and Physics*, *17*(15), 9665–9675. https://doi.org/10.5194/acp-17-9665-2017

Park, K., Kim, I., Choi, J.-O., Lee, Y., Jung, J., Ha, S.-Y., et al. (2019). Unexpectedly high dimethyl sulfide concentration in high-latitude Arctic sea ice melt ponds. *Environmental Science: Processes & Impacts*, *22*, 1642–1649. https://doi.org/10.1039/C9EM00195F

Qu, B., & Gabric, A. J. (2010). Using genetic algorithms to calibrate a dimethylsulfide production model in the Arctic ocean. *Chinese Journal of Oceanology and Limnology*, *28*(3), 573–582. https://doi.org/10.1007/s00343-010-9062-x

Qu, B., Gabric, A. J., Zeng, M., & Lu, Z. (2016). Dimethylsulfide model calibration in the Barents Sea using a genetic algorithm and neural network. *Environmental Chemistry*, *13*(2), 413–424. https://doi.org/10.1071/EN14264

Rempillo, O., Seguin, A. M., Norman, A.-L., Scarratt, M., Michaud, S., Chang, R., et al. (2011). Dimethyl sulfide air-sea fluxes and biogenic sulfur as a source of new aerosols in the Arctic fall. *Journal of Geophysical Research*, *116*, D00S04. https://doi.org/10.1029/2011JD016336

Riser, S. C., Freeland, H. J., Roemmich, D., Wijffels, S., Troisi, A., Belbéoch, M., et al. (2016). Fifteen years of ocean observations with the global Argo array. *Nature Climate Change*, *6*(2), 145–153. https://doi.org/10.1038/nclimate2872

Rutgers van der Loeff, M. M., Cassar, N., Nicolaus, M., Rabe, B., & Stimac, I. (2014). The influence of sea ice cover on air-sea gas exchange estimated with radon-222 profiles. *Journal of Geophysical Research: Oceans*, *119*, 2735–2751. https://doi.org/10.1002/2013JC009321

Schweiger, A., Lindsay, R., Zhang, J., Steele, M., Stern, H., & Kwok, R. (2011). Uncertainty in modeled Arctic sea ice volume. *Journal of Geophysical Research*, *116*, C00D06. https://doi.org/10.1029/2011JC007084

Shalina, E. V., & Sandven, S. (2018). Snow depth on Arctic sea ice from historical in situ data. *The Cryosphere*, *12*(6), 1867–1886.

Sharma, S., Chan, E., Ishizawa, M., Toom-Sauntry, D., Gong, S. L., Li, S. M., et al. (2012). Influence of transport and ocean ice extent on biogenic aerosol sulfur in the Arctic atmosphere. *Journal of Geophysical Research*, *117*, D12209. https://doi.org/10.1029/2011JD017074

Sim, R. (2001). Production of atmospheric sulfur by oceanic plankton: Biogeochemical, ecological and evolutionary links. *Trends in Ecology & Evolution*, *16*(6), 287–294.

Six, K. D., Kloster, S., Ilyina, T., Archer, S. D., Zhang, K., & Maier-Reimer, E. (2013). Global warming amplified by reduced sulphur fluxes as a result of ocean acidification. *Nature Climate Change*, *3*(11), 975–978. https://doi.org/10.1038/nclimate1981

Soltwedel, T., Bauerfeind, E., Bergmann, M., Bracher, A., Budaeva, N., Busch, K., et al. (2016). Natural variability or anthropogenically-induced variation? Insights from 15 years of multidisciplinary observations at the Arctic marine LTER site HAUSGARTEN. *Ecological Indicators*, *65*, 89–102. https://doi.org/10.1016/j.ecolind.2015.10.001

Stefels, J. (2000). Physiological aspects of the production and conversion of DMSP in marine algae and higher plants. *Journal of Sea Research*, *43*(3–4), 183–197. https://doi.org/10.1016/S1385-1101(00)00030-7

Stefels, J., Steinke, M., Turner, S., Malin, G., & Belviso, S. (2007). Environmental constraints on the production and removal of the climatically active gas dimethylsulphide (DMS) and implications for ecosystem modelling. *Biogeochemistry*, *83*(1–3), 245–275. https://doi.org/10.1007/s10533-007-9091-5

Steiner, N. S., Sou, T., Deal, C., Jackson, J. M., Jin, M., Popova, E., et al. (2015). The future of the subsurface chlorophyll-a maximum in the Canada basin—A model intercomparison. *Journal of Geophysical Research: Oceans*, *120*, 387–409. https://doi.org/10.1002/2015JC011232

Stroeve, J., & Notz, D. (2018). Changing state of Arctic sea ice across all seasons. *Environmental Research Letters*, *13*(10), 103001. https://doi.org/10.1088/1748-9326/aade56

Stroeve, J. C., Serreze, M. C., Holland, M. M., Kay, J. E., Malanik, J., & Barrett, A. P. (2012). The Arctics rapidly shrinking sea ice cover: A research synthesis. *Climatic Change*, *110*(3–4), 1005–1027. https://doi.org/10.1007/s10584-011-0101-1

Swart, N. C., Cole, J. N. S., Kharin, V. V., Lazare, M., Scinocca, J. F., Gillett, N. P., et al. (2019). The Canadian Earth system model version 5 (CanESM5.0.3). *Geoscientific Model Development*, *12*(11), 4823–4873. https://doi.org/10.5194/gmd-12-4823-2019

Tesdal, J.-E., Christian, J. R., Monahan, A. H., & von Salzen, K. (2016). Evaluation of diverse approaches for estimating sea-surface DMS concentration and air sea exchange at global scale. *Environmental Chemistry*, *13*(2), 390–412. https://doi.org/10.1071/EN14255

Thackeray, C. W., & Hall, A. (2019). An emergent constraint on future Arctic sea-ice albedo feedback. *Nature Climate Change*, *9*(12), 972–978. Number: 12 Publisher: Nature Publishing Group https://doi.org/10.1038/s41558-019-0619-1

Vancoppenolle, M., Bopp, L., Madec, G., Dunne, J., Ilyina, T., Halloran, P. R., & Steiner, N. (2013). Future Arctic Ocean primary productivity from CMIP5 simulations: Uncertain outcome, but consistent mechanisms. *Global Biogeochemical Cycles*, *27*, 605–619. https://doi.org/10.1002/gbc.20055

Wang, S., Elliott, S., Maltrud, M., & Cameron-Smith, P. (2015). Influence of explicit Phaeocystis parameterizations on the global distribution of marine dimethyl sulfide. *Journal of Geophysical Research: Biogeosciences*, *120*, 2158–2177. https://doi.org/10.1002/2015JG003017

Watanabe, E., Jin, M., Hayashida, H., Zhang, J., & Steiner, N. (2019). Multi-model intercomparison of the Pan-Arctic ice-algal productivity on seasonal, interannual, and decadal timescales. *Journal of Geophysical Research: Oceans*, *124*, 9053–9084. https://doi.org/10.1029/2019JC015100

Willis, M. D., Burkart, J., Thomas, J. L., Köllner, F., Schneider, J., Bozem, H., et al. (2016). Growth of nucleation mode particles in the summertime Arctic: A case study. *Atmospheric Chemistry and Physics*, *16*(12), 7663–7679. https://doi.org/10.5194/acp-16-7663-2016

Zahariev, K., Christian, J. R., & Denman, K. L. (2008). Preindustrial, historical, and fertilization simulations using a global ocean carbon model with new parameterizations of iron limitation, calcification, and N2 fixation. *Progress in Oceanography*, *77*(1), 56–82. https://doi.org/10.1016/j.pocean.2008.01.007

Zhang, J., & Rothrock, D. A. (2003). Modeling global sea ice with a thickness and enthalpy distribution model in generalized curvilinear coordinates. *Monthly Weather Review*, *131*(5), 845–861. https://doi.org/10.1175/1520-0493(2003)131<0845:MGSIWA>2.0.CO;2